NOAA Technical Memorandum ERL NSSL-88

THE RELATIONSHIP OF THE 300-MB JET STREAM TO TORNADO OCCURRENCE

Carolyn M. Kloth
Robert P. Davies-Jones

National Severe Storms Laboratory
Norman, Oklahoma
July 1980

UNITED STATES
DEPARTMENT OF COMMERCE
Philip M. Klutznick, Secretary

NATIONAL OCEANIC AND
ATMOSPHERIC ADMINISTRATION
Richard A. Frank, Administrator

Environmental Research
Laboratories
Wilmot N. Hess, Director

TABLE OF CONTENTS

LIST OF FIGURES

LIST OF TABLES

ABSTRACT

The relationship between the upper tropospheric jet stream and tornado occurrence was examined. The 300-mb wind field over the United States was analyzed and parameters such as divergence, relative vorticity, horizontal wind shear, and positive vorticity advection were computed. The data from May 1977 revealed that tornadoes generally occurred beneath stronger than average 300-mb winds of 15 to 30 m s^{-1}, within 1250 km of a 35 to 55 m s^{-1} jet streak, beneath the left front or right rear quadrant of the jet streak, and were generally of F0 or F1 intensity. Most tornadoes occurred beneath areas of 300-mb divergence, positive vorticity advection, and weak relative vorticity ($<4.8 \times 10^{-5}$ s^{-1}). Values of divergence and vorticity advection above the tornadoes were significantly positive with mean values of 1.8×10^{-5} s^{-1} and 19×10^{-10} s^{-2}, respectively. Horizontal wind shear at 300-mb was shown not to be a statistically significant variable in tornado occurrence. However, there was a tendency for weak tornadoes (F0) to be associated with anticyclonic shear while stronger tornadoes ($\geq$F1) tended to be associated with cyclonic shear. Four days were examined in detail in an effort to discover how and why the tornado situations differed. The strength and combination of the 300-mb parameters influenced tornado intensity and the pattern of tornado events.

THE RELATIONSHIP OF THE 300-MB JET STREAM TO TORNADO OCCURRENCE

Carolyn M. Kloth and Robert P. Davies-Jones

1. THE JET STREAM

1.1 Introduction

During the experimental high-level bombing raids in World War II, the pilots unexpectedly encountered winds over Japan with velocities sometimes reaching 100 m s^{-1} (Reiter, 1967). These strong winds created a baffling problem. If a bombing run was charted directly downwind, the bombs would overshoot their targets due to the excessive ground speed of the aircraft. If the approach was made directly upwind, the aircraft became nearly stationary over the target and were themselves in danger of becoming easy targets for ground-based defense. The "jet stream" encountered by the bombers was an important factor in forcing a change of tactics to low-level bombing raids.

The discovery of the jet stream in the mid-1940's introduced a feature of the circulation in the westerlies that was not included in any existing atmospheric models (Riehl et al., 1954). Since then, studies have been made on this significant feature and its interaction with other meteorological phenomena. It has been noted that jet streams influence severe storm development and, in particular, tornado occurrence. Many papers have been written in an attempt to understand how this influence manifests itself.

The purpose of this investigation is to explore the relationship between the upper tropospheric jet stream and tornado occurrence. Parameters such as wind speed, horizontal divergence, relative vorticity, vorticity advection, height tendencies, and horizontal wind shear are examined at the 300-mb level in an effort to elucidate the influence of the jet stream on tornado occurrence.

1.2 Discussion of the Jet Stream and Past Research

The jet stream is defined as a fast narrow current of air, near the tropopause, characterized by strong vertical and lateral wind shears. It is usually a few thousands of kilometers long, hundreds of kilometers wide, and a few kilometers deep (McIntosh, 1972). Currently, in the analysis of upper-level charts, a jet stream is indicated wherever it is reliably determined that the wind speed equals or exceeds 25 m s^{-1} (50 knots) (Huschke, 1959).

The location of the jet stream varies latitudinally with the season and the height of the strongest winds varies with both latitude and season. In view of this variation and the known tendency for the tropopause to shift to higher elevations with the advent of the warmer season, the 300-mb chart is considered the most suitable for representing the jet stream at high latitudes and in winter, and the 200-mb chart for low latitudes and in summer (Riehl et al., 1954).

The jet stream tends to flow along the isobars in the regions of steepest pressure gradient and, hence, undulates nearly parallel to the contours of the synoptic-scale troughs and ridges. The core of the jet stream is known to meander in the vertical as well as the horizontal direction. Examination of isotach analyses at more than one level, e.g., the 300-mb and 200-mb levels, often shows differences in maximum wind location due to the vertical undulations of the core (McNulty, 1978).

Along the axis of a well-developed jet stream, a succession of velocity maxima alternate with intervals where the winds are comparatively weak. These velocity maxima and minima are generally connected with the shortwave troughs in the westerlies and usually move downstream with a speed comparable to the phase speed of these troughs (Riehl et al., 1954).

It has been observed that severe weather events, particularly tornadoes, tend to occur frequently in the vicinity of these upper-tropospheric jet maxima, or jet streaks as they are otherwise called. Fawbush et al. (1951) pointed out the importance of high wind speeds aloft in severe storm and tornado outbreaks. Lee and Galway (1956) investigated flow characteristics at the 200-mb level and found a correspondence between the presence of a wind maximum at that level and tornado occurrence.

The rapid increases and decreases of wind speed along the direction of flow produce patterns of horizontal stretching and shrinking, i.e., divergence and convergence. In fact, the largest values of divergence in the upper troposphere are generally associated with the jet-level wind maxima (Newton and Palmén, 1963). This is important for severe weather production because horizontal divergence gives rise to significant synoptic-scale vertical motion. Upward motions decrease atmospheric stability as described below.

Beebe and Bates (1955) described a pattern of low-level horizontal convergence surmounted by horizontal divergence at some higher level. The result is an upward motion field sufficient to modify the environment from one of marked convective instability (with dry air aloft and an inversion-capped moist layer) to one of marked parcel instability (with moisture penetrating to greater heights and the elimination of the capping inversion). Hence, this pattern provides a favorable environment for the development of severe and tornadic thunderstorms. Since the largest values of upper-level divergence are generally associated with the strongest winds, a jet-level wind maximum is often associated with severe weather outbreaks.

In their paper, Beebe and Bates suggested that the areas of upper-level divergence were associated with the divergent quadrants of the jet streak (i.e., the left front and right rear quadrants) and that the lower-level convergence was associated with the left side of the low-level jet. The upper and lower-level jets combine to create the region of convective instability within which the severe weather ultimately develops. Uccellini and Johnson (1979) investigated more closely the coupling of the upper and lower-level jets. They noted the presence of a direct circulation in the entrance region of the upper-level jet streak and an indirect circulation in the exit region (Fig. 1). These circulations develop due to the large ageostrophic deviations of the wind which tend to be associated with the strongest winds

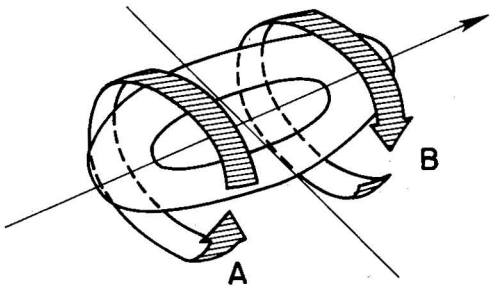

Figure 1. Idealized view of the direct (A) and indirect (B) circulations (secondary flow) in the vicinity of an upper-level jet streak. Small arrow indicates direction of primary flow. Closed contours are isotachs.

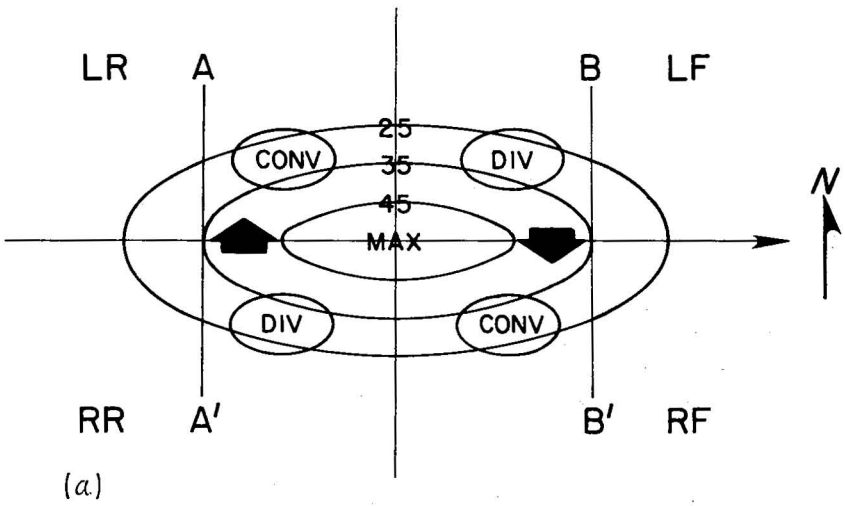

(a)

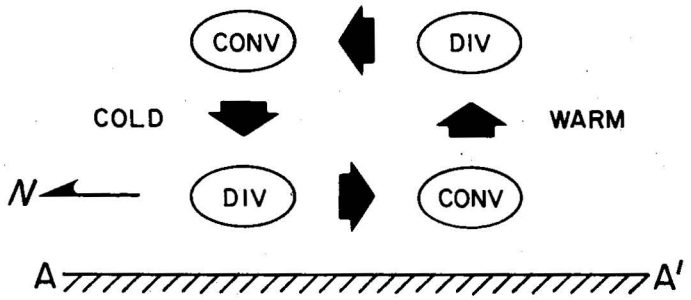

(b)

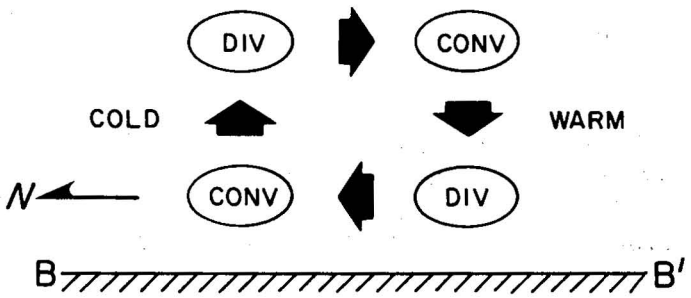

(c)

Figure 2(a). Patterns of ageostrophic motion and divergence near a jet streak in westerly flow. Isotachs are in m s^{-1}. Heavy black arrows indicate ageostrophic components of the wind. (b) Vertical cross-section through the entrance region (AA′) showing direct circulation. (c) Vertical cross-section through the exit region (BB′) showing indirect circulation (after Sechrist and Whittaker, 1979).

(Newton, 1959). In the entrance region of a jet "max" (Fig. 2a), as an air parcel accelerates toward the core, the ageostrophic wind component is directed toward the cyclonic side. This results in convergence in the left rear (LR) quadrant of the jet streak and divergence in the right rear (RR) quadrant. In the vertical (Fig. 2b), there is sinking motion beneath the LR quadrant and rising motion beneath the RR quadrant. The circulation that develops is thermally direct since cold air is sinking and warm air is rising. In the exit region (Figs. 2a and 2c), the reverse is true. The ageostrophic component is directed toward the anticyclonic side, resulting in convergence in the right front (RF) quadrant and divergence in the left front (LF) quadrant. Here, the vertical circulation is thermally indirect since warm air is sinking and cold air is rising.

Uccellini and Johnson (1979) observed that when the upper and lower-level jets were analyzed on isentropic surfaces, the two apparently distinct features appeared to merge; i.e., the lower-level jet was embedded in the return branch of the indirect circulation associated with the upper-level jet. Hence, the so-called low-level jet that is often observed at 850 mb, particularly in the spring, may actually be a downward extension of the upper-tropospheric jet stream. This was noted previously by Riehl et al. (1954) and more recently by Horn and Achtor (1979). Sechrist and Whittaker (1979) further expanded the idea of implied vertical circulations. Using the theory of mass adjustment, they examined the distribution of speed changes in the vicinity of a jet streak by computing the height advection at 300 mb. Sechrist and Whittaker also examined the divergence field at 300 mb and found that the divergence patterns previously assumed to exist in the vicinity of a jet streak (e.g., those postulated by Riehl et al., 1954, and Beebe and Bates, 1955) actually are observed in the atmosphere.

McNulty (1978) investigated the relationship between divergence in the 300-200-mb layer and severe weather occurrence. He noted that divergence was present in this layer during severe weather, but that the majority of tornadoes in his study occurred with moderate to weak divergence values (less than 2.5×10^{-5} s^{-1}). McNulty proposed that either an upper tropospheric jet stream or a shortwave trough, or more frequently, the combination of the two features are the main cause of upper-level divergence associated with severe weather outbreaks.

Shortwave troughs are associated with upper-level divergence for the following reason. On the leading edge of an approaching shortwave trough is an area of positive vorticity advection (PVA). Divergence is associated with areas of PVA as shown below. Following Hales (1979), consider the vorticity equation in (x,y,p,t) coordinates:

$$\frac{d\eta}{dt} = \frac{\partial \eta}{\partial t} + \vec{V} \cdot \nabla \eta + \omega \frac{\partial \eta}{\partial p} = -\eta D + \text{other terms}, \qquad (1)$$

where $\vec{V}$ is the wind vector, ∇ is the horizontal Laplacian, η is absolute vorticity, D is horizontal divergence, and $\omega = \frac{dp}{dt}$ (the analogous quantity in pressure coordinates to vertical velocity in height coordinates). The "other terms" are the twisting and frictional terms which are small compared to divergence on the synoptic scale. If we neglect vertical advection

and the other terms, as is done in the quasi-geostrophic vorticity equation, and assume a steady state, (1) can be simplified to

$$\frac{-\vec{V}\cdot\nabla\eta}{\eta} \simeq D \quad . \tag{2}$$

Recall that η is almost always positive and PVA is defined as PVA $= -\vec{V}\cdot\nabla\eta$, so to a first approximation (i.e., to the extent that dropping the $\frac{\partial\eta}{\partial t}$ term is justified), areas of PVA are divergent and areas of negative vorticity advection (NVA) are convergent. Neglecting the other terms on the right hand side of (1) yields

$$\frac{1}{\eta}\frac{d\eta}{dt} = \frac{d\ \ln\ \eta}{dt} = -D \quad .$$

Thus, divergence is associated with decreasing absolute vorticity of air parcels.

The above can be applied to jet streaks and helps to explain the associated divergence patterns. Consider a straight jet streak. Since there is no curvature, the only contribution to vorticity is from shear vorticity. As shown in Fig. 3a, there is a vorticity maximum on the left side of the jet streak with PVA downstream (LF quadrant) and NVA upstream (LR quadrant). On the right side of the jet streak, there is a vorticity minimum with NVA downstream (RF quadrant) and PVA upstream (RR quadrant). Employing the argument relating divergence and PVA, the pattern of divergence near a jet streak should be as shown in Fig. 3b. For air flowing through a trough (Fig. 3c), the main contribution to vorticity is from curvature vorticity. There will be a vorticity maximum at the base of the trough with PVA ahead of it and NVA behind it. When a jet streak coincides with a trough (Fig. 3d), shear vorticity and curvature vorticity are both appreciable. The PVA-NVA couplet on the left side of the jet streak will be enhanced by the PVA-NVA couplet associated with the trough while the NVA-PVA couplet on the right side of the jet streak will be weakened. Thus, for a cyclonically curved jet streak, divergence can be inferred only in the LF quadrant of the jet streak and convergence only in the LR quadrant, as shown in Fig. 3e. The opposite is true for an anticyclonically curved jet streak. As shown in Fig. 3f, there is divergence in the RR quadrant and convergence in the RF quadrant.

The relationship between PVA and vertical motion can be established through consideration of the quasi-geostrophic omega equation (Holton, 1972):

$$\left[\nabla^2 + \frac{f_o^2}{\sigma}\frac{\partial^2}{\partial p^2}\right]\omega = \frac{f_o}{\sigma}\frac{\partial}{\partial p}\left[\vec{V}_g\cdot\nabla\eta_g\right] + \frac{1}{\sigma}\nabla^2\left[\vec{V}_g\cdot\nabla\left[\frac{-\partial\Phi}{\partial p}\right]\right] \quad , \tag{3}$$

where f_o is the Coriolis parameter, σ is the static stability parameter, Φ is the geopotential ($\frac{-\partial\Phi}{\partial p}$ is the vertical gradient of the geopotential), η_g is geostrophic absolute vorticity, and $\vec{V}_g$ is the geostrophic wind vector.

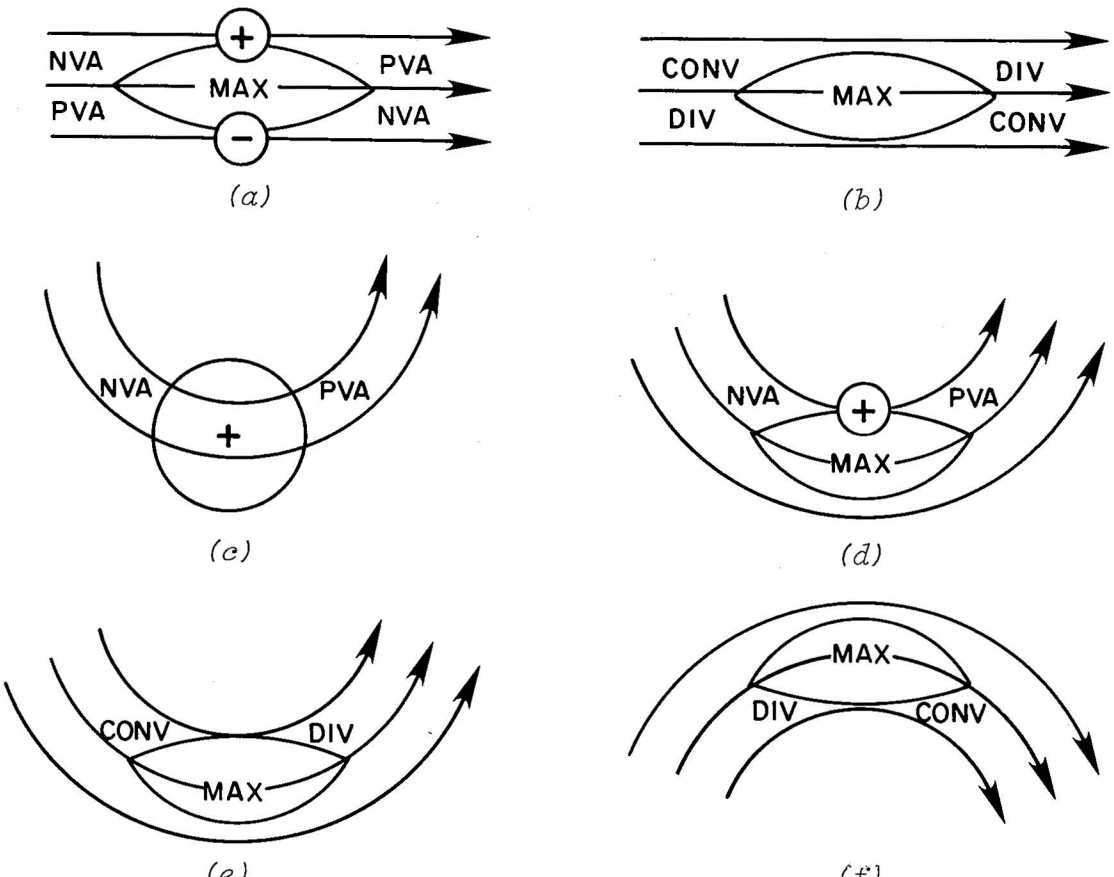

Figure 3. Configurations of jet streaks in westerly flow: (a) straight jet with distribution of shear vorticity; (b) divergence pattern inferred from (a); (c) air flow through a trough with distribution of curvature vorticity; (d) jet streak coincident with trough showing distribution of vorticity; (e) cyclonically curved jet streak with divergence pattern inferred from (d); (f) anticyclonically curved jet streak with associated divergence pattern. Closed contours indicate isotachs.

The thickness advection term is generally smaller than the differential PVA term at upper levels since isotherms and contours tend to coincide. Thus, (3) may be simplified to the following form:

$$\left[\nabla^2 + \frac{f_o^2}{\sigma}\frac{\partial^2}{\partial p^2}\right]\omega \simeq \frac{f_o}{\sigma}\frac{\partial}{\partial p}\left[\vec{V}_g \cdot \nabla\eta_g\right] \quad . \tag{4}$$

At upper levels, $\vec{V} \simeq \vec{V}_g$ and $\eta \simeq \eta_g$. Note that $\left[\nabla^2 + \frac{f_o^2}{\sigma}\frac{\partial^2}{\partial p^2}\right]\omega \propto -\omega$ (Holton, 1972), $\omega = -\rho g w$, and $\frac{\partial}{\partial p} \propto -\frac{1}{\rho g}\frac{\partial}{\partial z}$. Equation (4) can be rewritten as

$$w \propto \frac{\partial}{\partial z}\left[-\vec{V}\cdot\nabla\eta\right] \quad .$$

Note that upward motion is proportional to the vertical increase of PVA, not just to PVA itself.

We can elucidate the above relationships further if we consider height tendencies. The relationship between PVA and the height tendency can be established through the quasi-geostrophic height tendency equation

$$\left[\nabla^2 + \frac{f_o^2}{\sigma}\frac{\partial^2}{\partial p^2}\right]\chi = f_o\left[-\vec{V}_g\cdot\nabla\eta_g\right] + \frac{f_o^2}{\sigma}\frac{\partial}{\partial p}\left[-\vec{V}_g\cdot\nabla\left(\frac{\partial\Phi}{\partial p}\right)\right] \quad , \qquad (5)$$

where $\chi = \frac{\partial\Phi}{\partial t}$ is the geopotential tendency (Holton, 1972). Considering only the PVA term (i.e., omitting the thickness advection term) we have

$$\left[\nabla^2 + \frac{f_o^2}{\sigma}\frac{\partial^2}{\partial p^2}\right]\chi \simeq f_o\left[-\vec{V}_g\cdot\nabla\eta_g\right] \quad . \qquad (6)$$

Since $\vec{V} \simeq \vec{V}_g$, $\eta \simeq \eta_g$, and $\left[\nabla^2 + \frac{f_o^2}{\sigma}\frac{\partial^2}{\partial p^2}\right]\chi \propto -\chi$, PVA regions tend to be associated with height falls and NVA regions with height rises.

In summary, areas of PVA typically are divergent and are associated with height falls; when PVA increases with height there is generally upward motion.

Significant areas of divergence can also be found in diffluent patterns. House (1958) observed that areas of strong divergence aloft were not necessarily associated with wind maxima but were characterized by large streamline diffluence. Lee and Galway (1958) agreed, stating that areas of horizontal divergence could be associated with both speed divergence in the vicinity of the jet stream and diffluent patterns with weak flow and markedly diverging streamlines. Karst (1977) and Whitney (1977) both showed, in separate studies, that the diffluent area between the polar and subtropical jet streams provided a favorable region for severe thunderstorm development. This is important in those situations (e.g., the warm season) that are not associated with obvious jet maxima, but where the major source of upper-level divergence is from diffluent flow. A quantitative calculation of divergence would be helpful in identifying the less obvious but nevertheless significant areas of divergence.

Although it has been established that upper-level divergence plays an important part in severe storm development, there are cases where severe storm complexes apparently have altered the synoptic-scale flow, causing enhancement of the divergence aloft. Maddox (1979) showed in his analysis of an intense convective storm complex that the upper-level flow was significantly modified by the storms. He noted that the strong diffluence observed over the meso-α scale[1] storm complex and the intensification of the jet streak along its northern edge were in response to the growth and organization of the complex rather than the cause of its development.

---

[1] The meso-α scale characteristic length is on the order of 100 to 1000 kilometers.

The aforementioned parameters (divergence, vorticity advection, height tendency, and strong wind maxima) are all important in the upper troposphere for severe thunderstorm development. However, there is another important factor, horizontal wind shear, that has been considered previously. The greatest cyclonic and anticyclonic shears are located at the jet stream level due to the rapid decrease of wind speed on either side of the jet stream core. Hales (1979) claimed that anticyclonic shear areas appear to be associated with tornadoes (and other severe weather) more frequently than cyclonic shear areas. This may be due to the usually closer proximity of the anticyclonic shear side of a jet streak to warm, moist low-level air, or due to the connection between divergence and decreasing absolute vorticity, and hence in time with low values of absolute vorticity.

To the right of the jet core, the negative relative vorticity due to anticyclonic shear is almost equal to the Coriolis parameter in magnitude (Petterssen, 1956). On the large scale, the absolute vorticity, η, is always greater than or equal to zero and the atmosphere is inertially stable. However, η can be negative (i.e., $-\zeta > f$) near jet streams over small areas. This produces inertial instability which some (e.g., Miller, 1972; Emanuel, 1978) think may be helpful in triggering severe weather.

2. METHODS OF EVALUATING RELATIONSHIPS BETWEEN TORNADOES AND THE 300-MB JET STREAM

2.1 Discussion of the Data

The 300-mb data in this study were obtained from a National Severe Storms Forecast Center (NSSFC) Raob History tape. This magnetic tape contains the twice daily (0000 and 1200 GMT) sounding data from all the United States National Weather Service (NWS) stations as well as Canadian and Mexican stations. For this study, 300-mb data from 71 NWS stations, plus two Mexican stations (Empalme and Chihuahua) were used.

The tornado information (location, time of occurrence, etc.) was obtained from Storm Data (U.S. Department of Commerce, 1977c) and the Severe Local Storms Unit (SELS) log. The SELS log is a tape of confirmed severe weather events maintained by NSSFC.

Only those tornadoes that occurred in the Great Plains (i.e., those states east of the Rocky Mountains and west of the Mississippi River, plus Wisconsin and Illinois) were considered. This 17-state, 4×10^6 km^2 sub-area (test region) was selected because it is the area where tornadoes generally occur. The month of May 1977 (during which 207 tornadoes were confirmed within this area) was chosen because this period provided a representative data set which was a reasonable size for this investigation.

May is the most active tornado month in the United States averaging 155 tornadoes and 25 tornado-related deaths (U.S. Department of Commerce, 1977a). May 1977 was more active than usual with 228 tornadoes across the United States, but only four tornado deaths occurred. The above normal tornado

activity may be attributed to a deep mean upper-level trough on the west coast of North America and mean southwesterly flow aloft across the Great Plains (Dickson, 1977).

Of the 207 tornadoes, 58 were neglected because they did not occur within 3 hours (plus or minus) of map time, and the data was considered unrepresentative of the synoptic-scale environment at tornado time. Six additional tornadoes were neglected due to lack of data for two of the days (25 and 31 May) in May 1977. All the remaining 143 tornadoes occurred between 2100 GMT and 0300 GMT rather than between 0900 GMT and 1500 GMT.

Extensive use was made of the SUPMAP computer subroutine developed at the National Center for Atmospheric Research (NCAR). This subroutine generates a map of the United States from any one of nine projections. All maps in this study are polar stereographic projections, true at ninety degrees North latitude.

2.2 Description of the Evaluation Methods

2.2.1 Preliminary Statistics

As an initial step toward understanding the relationship between the 300-mb jet stream and tornado occurrence, the statistics of the 300-mb winds in the vicinity of tornadoes are examined. Questions, such as what wind speeds are generally associated with tornado occurrences, where is the jet streak generally located relative to a tornado, and how strong are the winds associated with the jet streak, are addressed.

To help answer these questions a map of tornado occurrences was generated for each day from the SELS data. On this map was superimposed the corresponding National Meteorological Center (NMC) 300-mb facsimile chart with isotach patterns and station wind data. For each tornado, the following quantities were noted: 1) the wind speed (m s^{-1}) directly above the tornado, 2) the wind speed (m s^{-1}) at the core of the 300-mb jet streak, 3) the distance (km) of the tornado from the jet core, 4) the quadrant of the jet streak beneath which the tornado occurred, and 5) the F scale intensity of the tornado (Fujita, 1971).

Since NMC labels the isotachs every 20 knots (i.e., every 10 m s^{-1}), the wind speed was categorized by intervals such as 0-5 m s^{-1}, 5-15 m s^{-1}, 15-25 m s^{-1}, etc. A jet streak was defined as having a closed isotach of at least 25 m s^{-1}. The maximum wind speed in the jet core was estimated as the value of the innermost isotach plus 10 m s^{-1}. The centroid of the innermost isotach was chosen as the jet core location. If there was more than one jet "max," then the one closest to the tornado activity was used.

The distance of the tornado from the jet core was determined using a simple mathematical expression involving σ, the image scale factor, and m, the map scale factor. Sigma, defined as the ratio of image plane distance to earth distance, is given for a polar stereographic map by $\sigma = (1 + \sin \phi_0)/(1 = \sin \phi)$, where ϕ_0 is the reference latitude and ϕ is the latitude of the point under consideration (Saucier, 1956). In actuality, since the jet core

and the tornado were usually at different latitudes, ϕ_1 and ϕ_2, an average latitude, $\overline{\phi} = (\phi_1 + \phi_2)/2$, was used in distance computations. The map scale factor, m, is defined as m = map distance/image plane distance. For the polar stereographic map used here, m = 1/20,600,000 for $\phi_o = 90°$. The conversion from map distance to earth distance was accomplished using the following expression:

$$L_e = \frac{L_m}{m \cdot \sigma} \times 10^{-5}$$

where L_e is earth distance (km) and L_m is map distance (cm).

2.2.2 Isotachs and Streamlines

Isotach and streamline analyses at the 300-mb level were performed for both 1200 and 0000 GMT on each tornado day. For the Great Plains region, local standard time (CST) is six hours behind Greenwich Mean Time (GMT). The 0000 GMT maps are the most important since the tornadoes occurred near this time.

The isotach analysis was achieved by objectively analyzing the wind speed from each station onto a 17 x 11 grid (see Appendix A for a discussion of the objective analysis routine). The streamline analysis was obtained from objective analyses of the u and v components of the wind (i.e., those components directed along the x- and y-axes, respectively).

Two plotting routines, available at the National Severe Storms Laboratory (NSSL), were utilized to construct contours and streamlines (Achtemeier, 1979).

2.2.3 Divergence and Vorticity

The 300-mb divergence and relative vorticity fields were computed for both 1200 and 0000 GMT on each tornado day. This was accomplished by first objectively analyzing the u/σ and v/σ fields (instead of just the u and v fields) since divergence is given by

$$DIV = \sigma^2\left[\frac{\partial}{\partial x}\left(\frac{u}{\sigma}\right) + \frac{\partial}{\partial y}\left(\frac{v}{\sigma}\right)\right] \quad , \tag{7}$$

and relative vorticity by

$$\xi = \sigma^2\left[\frac{\partial}{\partial x}\left(\frac{v}{\sigma}\right) - \frac{\partial}{\partial y}\left(\frac{u}{\sigma}\right)\right] \quad . \tag{8}$$

Centered finite differencing was used to compute the derivatives in the x- and y-directions. For divergence, the derivatives are

$$\frac{\partial}{\partial x}\left(\frac{u}{\sigma}\right) = \frac{\left(\frac{u}{\sigma}\right)_{i+1,j} - \left(\frac{u}{\sigma}\right)_{i-1,j}}{2\Delta x} \quad ,$$

and

$$\frac{\partial}{\partial y}\left(\frac{v}{\sigma}\right) = \frac{\left(\frac{v}{\sigma}\right)_{i,j+1} - \left(\frac{v}{\sigma}\right)_{i,j-1}}{2\Delta y} \quad ,$$

where i and j are grid point labels directed in the positive x- and y-directions, respectively, and Δx and Δy are the grid spacing in the x-and y-directions (here, $\Delta x = \Delta y$). Similar finite differences were used in the relative vorticity computation.

2.2.4 Horizontal Wind Shear

The horizontal wind shear in a natural coordinate system (s,n) is defined as $-\frac{\partial \vec{V}_s}{\partial n}$ where $\vec{V}_s = (V_s,0)$ is the wind vector (directed along the positive s direction) and n is distance perpendicular to the flow and increases to the left of the direction of motion (see Fig. 4). A translation of axes must be performed to change from the natural coordinate system to the x-y Cartesian coordinate system used in this study.

From Fig. 4

$$V_s = u \cos\theta + v \sin\theta \quad , \tag{9}$$

where θ is the angle between the x-axis and the vector $\vec{V}_s$, measured positively in the counterclockwise direction.

From elementary calculus and Fig. 5

$$\frac{\partial V_s}{\partial n} = \frac{\partial V_s}{\partial x}\frac{\partial x}{\partial n} + \frac{\partial V_s}{\partial y}\frac{\partial y}{\partial n} \quad ,$$

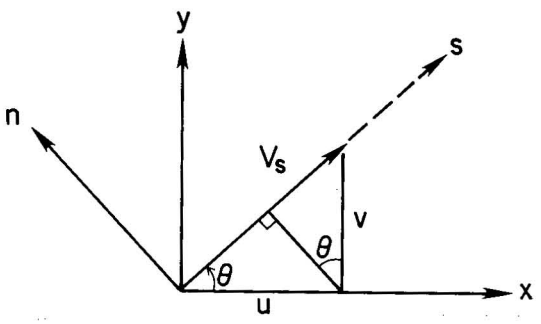

Figure 4. Relationship between the natural coordinate system (s,n) and the Cartesian coordinate system (x,y). V_s is the wind vector, θ is the angle between V_s and the x-axis, and u and v are the wind components in the x- and y-directions, respectively.

i.e.,

$$\frac{\partial V_s}{\partial n} = - \frac{\partial V_s}{\partial x} \sin \theta + \frac{\partial V_s}{\partial y} \cos \theta \quad . \tag{10}$$

By differentiating (9) with respect to x and with respect to y (keeping θ constant), we obtain the following

$$\frac{\partial V_s}{\partial x} = \frac{\partial u}{\partial x} \cos \theta + \frac{\partial v}{\partial x} \sin \theta \quad , \tag{11}$$

and

$$\frac{\partial V_s}{\partial y} = \frac{\partial u}{\partial y} \cos \theta + \frac{\partial v}{\partial y} \sin \theta \quad . \tag{12}$$

Substituting (11) and (12) into (10) yields the following expression for horizontal shear:

$$- \frac{\partial V_s}{\partial n} = (\frac{\partial u}{\partial x} - \frac{\partial v}{\partial y}) \cos \theta \sin \theta - \frac{\partial u}{\partial y} \cos^2 \theta + \frac{\partial v}{\partial x} \sin^2 \theta \quad . \tag{13}$$

The routine that computes the 300-mb horizontal wind shear first objectively analyzes the u and v components of the wind. The wind speed, V_s, and the sine and cosine of θ are then calculated directly from

$$V_s = (u^2 + v^2)^{1/2}, \quad \cos \theta = u/V_s, \text{ and } \sin \theta = v/V_s \quad .$$

Finally, the value of horizontal wind shear at each grid point is computed from (13), using centered finite differencing to evaluate the derivatives as before.

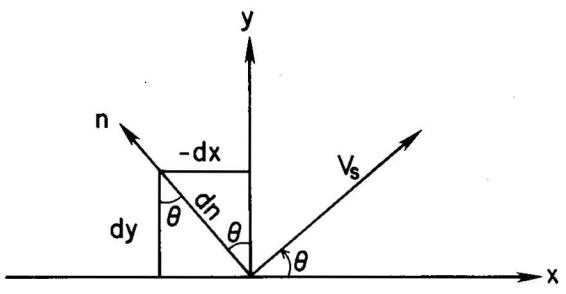

Figure 5. Conversion from the natural coordinate system to the x-y Cartesian coordinate system; dx and dy are the distances along the x- and y-axis, respectively, and dn is distance along the n-axis.

2.2.5 Height Tendencies

The 300-mb height tendency field was analyzed for both 1200 and 0000 GMT on each tornado day. This was done by first computing the height tendency, Δz, at each station using the following expression:

$$\Delta z(t - 6 \text{ hrs}) = z(t) - z(t - 12 \text{ hrs}) \quad ,$$

where $z(t)$ is the height of the 300-mb pressure surface in tens of meters at time t and Δz is the height tendency in tens of meters. The values at each station were then objectively analyzed onto a 17 x 11 grid. If Δz could not be computed for a given station because of missing data, no value was passed to the objective analysis routine for that location.

Note that the height tendency fields are actually valid for 1800 and 0600 GMT rather than for 0000 and 1200 GMT because Δz is centered midway through the 12-hour period, not at either the beginning or end of the period. Hence, these analyses do not portray the actual height tendencies which existed near tornado time.

2.2.6 Positive Vorticity Advection

Positive vorticity advection (PVA) is defined as

$$PVA = -\vec{V} \cdot \nabla_h(\xi + f) \quad , \tag{14}$$

where $\vec{V}$ is the wind vector, ∇_h is the horizontal Laplacian, ξ is the relative vorticity, and f is the earth's vorticity.

The 300-mb PVA field was analyzed for both 1200 and 0000 GMT sounding times. This was accomplished by objectively analyzing the u and v fields, the relative vorticity field (same as in Section 2.2.3), and by computing the earth's vorticity at each grid point. The following expression was used to compute PVA:

$$PVA = \sigma\left(-u \frac{\partial \xi}{\partial x} - v \frac{\partial \xi}{\partial y} - v \frac{\partial f}{\partial y}\right) \quad . \tag{15}$$

The horizontal derivatives were again computed using centered finite differences.

2.2.7 Other Influences

Some consideration must be given to influences below 300 mb since without favorable low-level conditions, even the most intense upper-level jets are unlikely to produce tornadic thunderstorms. Composite maps were constructed for each tornado day showing the 1200 GMT location of surface fronts, moist tongues and low-level jets at 850 mb, and the axes of shortwave

troughs at 500 mb. Fawbush et al. (1951), Miller (1972), and others agree that these features play important roles in the production of severe weather which may occur occasionally even when a 300-mb jet streak is absent. Atmospheric instability though not considered here, is also an important factor in severe weather development.

The position of the surface fronts was obtained from "Daily Weather Maps" (U.S. Department of Commerce, 1977b) which is published weekly. The 850-mb and 500-mb data were obtained from the appropriate 1200 GMT NMC facsimile charts.

The 1200 GMT data, rather than the 0000 GMT data, is presented since it was readily available for each day. Also, only the 1200 GMT data is available to a forecaster who is analyzing a typical potential tornado situation.

3. EXAMINATION AND INTERPRETATION OF THE ANALYSES AND SELECTED CASES

3.1 Results of the Preliminary Statistics

Figure 6 is a histogram of the 300-mb wind speeds directly above the tornadoes. The mean and standard deviation of this wind speed distribution are 23.3 m s^{-1} and 7.6 m s^{-1}, respectively. The most preferred wind speed interval was 15-25 m s^{-1} with 52% of the tornadoes occurring beneath winds of this speed. Eighty-four percent of the tornadoes happened below winds of 15-35 m s^{-1} and the winds were in excess of 35 m s^{-1} above only 6% of the

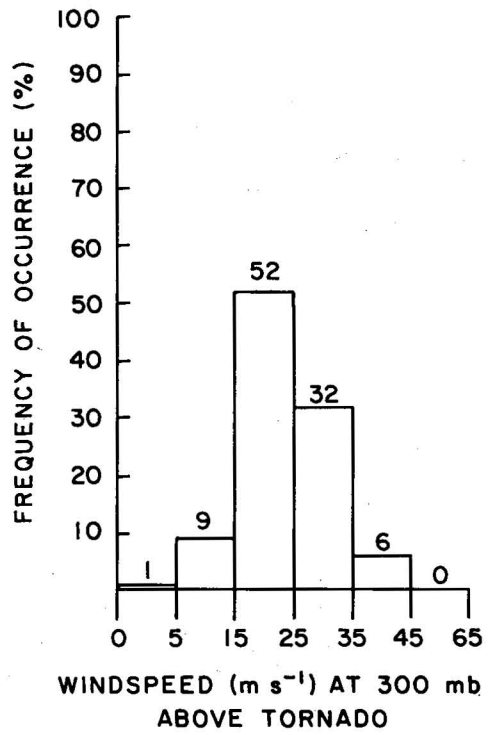

Figure 6. Histogram of the 300-mb wind speed (m s^{-1}) above each tornado (based on 143 tornadoes that occurred at 0000 GMT ±3 hours).

tornadoes. Based on accepted tornado forecasting criteria, one might expect the average tornado to be associated with a stronger 300-mb wind speed than 23 m s^{-1}. One thing to keep in mind, however, is the overall frequency of occurrence of the stronger wind speeds during May 1977. Were they a rare occurrence? Figure 7 shows the frequency of occurrence of wind speeds throughout the Great Plains region for May 1977. This histogram was constructed by tabulating the 300-mb winds from all 31 stations in the test region for the entire month (excluding 0000 GMT, 26 May, and 0000 GMT, 1 June, for which data is missing), utilizing both 0000 and 1200 GMT soundings. The figure shows that nearly 90% of the winds ranged between 5 m s^{-1} and 35 m s^{-1} while only 6% exceeded 35 m s^{-1} and none exceeded 55 m s^{-1}. Hence, the stronger wind speeds were indeed rare over the region of interest for May 1977. The mean and standard deviation of the 300-mb winds were 18.5 and 10.0 m s^{-1}, respectively.

A chi-square goodness of fit test (Yamane, 1973) on the data in Figs. 6 and 7 showed that the hypothesis that the 300-mb wind speeds above tornadoes have the same distribution as the wind speeds throughout the test region can be rejected at the .01 level of significance. Inspection of the data reveals that tornadoes tend to occur below higher than average wind speeds.

Figure 8, a histogram of the maximum wind speed of the jet core, shows that 52% of the tornadoes were associated with a jet whose core had winds of

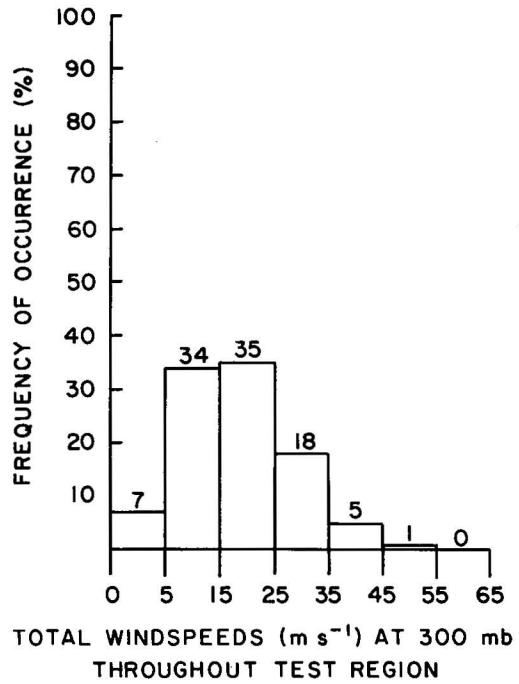

Figure 7. Histogram of the 300-mb wind speeds (m s^{-1}) for May 1977 throughout the Great Plains test region (based on 1,744 observations taken at 0000 and 1200 GMT, excluding 0000 GMT 26 May and 0000 GMT 1 June).

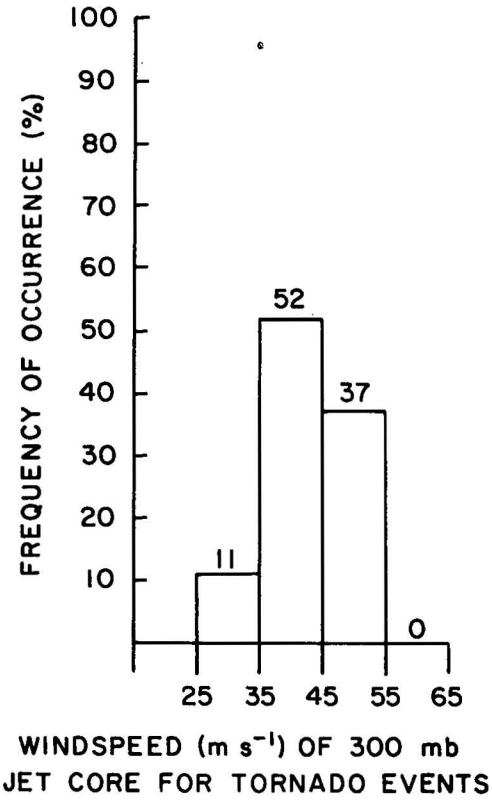

Figure 8. Histogram of the wind speed (m s^{-1}) of the 300-mb jet core associated with each tornado (based on 143 tornadoes).

35-45 m s^{-1}, and nearly 90% were associated with a jet whose maximum winds ranged between 35 m s^{-1} and 55 m s^{-1}. This is not unexpected since Table 1 shows that almost all of the jet cores for the entire month of May 1977 at 0000 GMT (excluding 1 June) had maximum winds between 35 m s^{-1} and 55 m s^{-1}. There were no jets in excess of 55 m s^{-1} over the United States during May. The distribution of wind speed maxima in Fig. 8 has a mean of 42.6 m s^{-1} and a standard deviation of 7.7 m s^{-1}. Table 1 also shows no significant dependence of the number of tornadoes per day on the strength of the jet core.

Table 1. Relationship between the number of tornadoes per day and the wind speed of the 300-mb jet streak for May 1977 at 0000 GMT (excluding 1 June 1977).

	WIND SPEED AT 300-MB JET CORE (0000 GMT) 25-35	35-45	45-55	TOTAL
Number of Days	2	16	12	30
Number of Tornadoes	16	74	53	143
No. of Tornadoes/Day	8	4.6	4.4	4.8

Figure 9 is a histogram of the distance of the tornado from the center of the jet streak. Over 50% of the tornadoes occurred between 625 km and 1250 km from the jet "max". Twenty-four percent of the tornadoes occurred at 625 km or less from the center of the jet streak while 20% occurred at distances greater than 1250 km. The distribution of distance of the tornado from the jet center has a median of 885 km, a mean of 937 km, and standard deviation of 434 km.

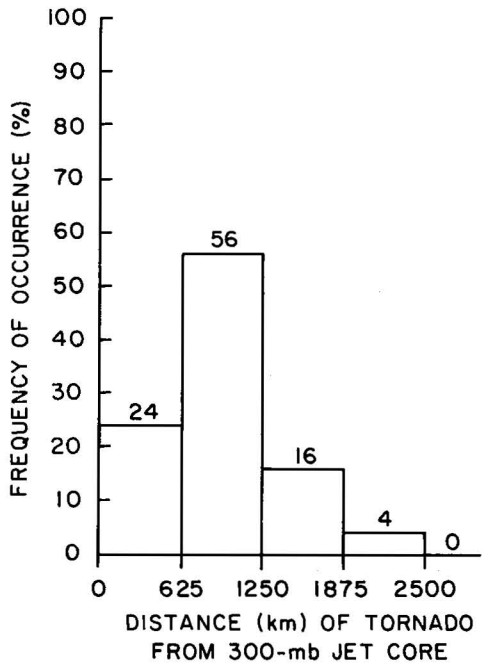

Figure 9. Histogram of the distance (km) of each tornado from the 300-mb jet core (based on 143 tornadoes).

Figure 10 shows the frequency of tornadoes per unit area as a function of distance from the jet streak center. The area normalization removes the inherent bias in Fig. 9 arising from outlying adjacent range circles encompassing more area than equally spaced ones closer to the center. The per unit area tornado frequency is a maximum in the 250-500 km range. Part of the fall-off in frequency as distance increases beyond 500 km is due to the range circles expanding beyond the boundaries of the test region, which has the same area as a circle with radius 1127 km.

This brings up an interesting question, namely, does the strength of the jet streak relate to the distance of the tornado from the center of the jet streak? Table 2 contains the relevant frequency data, which represents actual occurrences, not percentages. A chi-square test for independence (Yamane, 1973) reveals no significant correlation at the five percent level. For test purposes, the data had to be retabulated because of a rule that the expected frequencies, E_{jk}, should exceed 5. Even with the retabulation, it was not possible to satisfy this rule, but this test (and others discussed later in this section) are still believed to be significant because the cells with low E_{jk} contributed little to the overall chi-square score.

Table 3 shows the expected damage for each of six main F categories. The F scale was proposed by Fujita (1971) as a means to categorize tornadoes by their apparent intensity based on rough damage assessments. Tables 4 through 7 relate the F scale intensity of the tornadoes to some of the characteristics of jet streaks already mentioned. Seventy-eight of the 143 tornadoes under investigation belonged to the weakest category (F0), and only 25 were of F2 or greater intensity.

Table 4 compares the F scale of each tornado with the wind speed directly above it. The more intense tornadoes (F3 or greater) occurred beneath winds of 15-45 m s^{-1}, with 15-25 m s^{-1} the most preferred wind speed interval. This is surprising as one would expect the more intense tornadoes to occur beneath the stronger winds. A chi-square test fails to show any significant association between tornado intensity and overlying 300-mb wind speed.

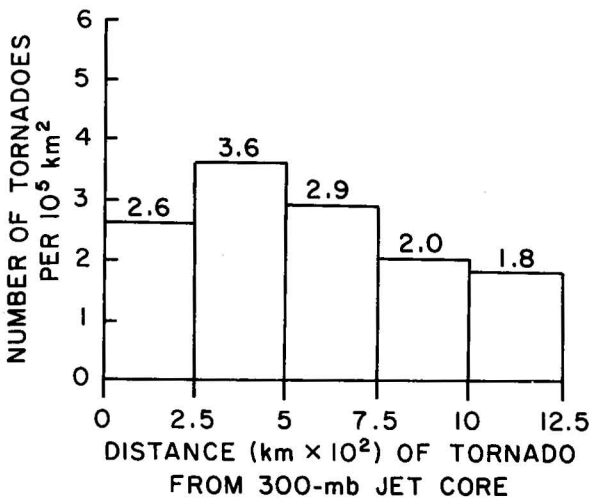

Figure 10. Frequency of tornadoes per unit area as a function of the distance from the jet streak center (based on 143 tornadoes).

Table 2. *Number of tornado occurrences as a function of distance (km) of tornado from the 300-mb jet core and wind speed (m s^{-1}) of the jet core (based on 143 tornadoes at 0000 GMT ±3 hours).*

	WINDSPEED AT JET CORE (m s^{-1})				
	25-35	35-45	45-55	55-65	TOTAL
0-625	3	20	11	0	34
626-937	1	25	17	0	43
938-1250	9	19	9	0	37
1251-1875	3	10	10	0	23
1876-2500	0	0	6	0	6
TOTAL	16	74	53	0	143

Table 3. *Expected wind damage for each F scale category (after Fujita, 1971).*

FUJITA SCALE FOR DAMAGING WIND	
SCALE	EXPECTED DAMAGE
F0	LIGHT DAMAGE - some damage to chimneys and TV antennae
F1	MODERATE DAMAGE - some roof damage, trees uprooted, light trailers pushed or over-turned
F2	CONSIDERABLE DAMAGE - roofs torn off, mobile homes destroyed
F3	SEVERE DAMAGE - some walls of well-built homes left standing
F4	DEVASTATING DAMAGE - no walls standing, rubble on foundation
F5	INCREDIBLE DAMAGE - foundations swept clean of rubble

Table 4. Statistical breakdown of tornado occurrences by wind speed ($m\ s^{-1}$) at 300 mb above the tornado and F scale (based on 143 tornadoes).

	F SCALE						
	F0	F1	F2	F3	F4	F5	TOTAL
0-5	1	0	0	0	0	0	1
5-15	8	4	1	0	0	0	13
15-25	43	19	4	4	4	1	75
25-35	25	14	4	2	0	0	45
35-45	1	3	4	1	0	0	9
TOTAL	78	40	13	7	4	1	143

Table 5. Breakdown of tornado occurrences by wind speed ($m\ s^{-1}$) of 300-mb jet core and F scale (based on 143 tornadoes).

	F SCALE						
	F0	F1	F2	F3	F4	F5	TOTAL
25-35	11	1	0	4	0	0	16
35-45	38	20	9	3	4	0	74
45-55	29	19	4	0	0	1	53
TOTAL	78	40	13	7	4	1	143

Table 5 compares the F scale of each tornado with the wind speed at the jet core. The data shows that most of the tornadoes were associated with the stronger jet cores. However, statistical analysis finds no evidence for any correlation between the tornado intensity and the wind speed of the jet core.

Table 6 compares the F scale with the distance of the tornado from the jet core. The data reveals no obvious relationship between the two, and a chi-square test supports this conclusion.

Table 6. Breakdown of tornado occurrences by distance (km) of the tornado from the 300-mb jet core and F scale (based on 143 tornadoes).

	F SCALE						
	F0	F1	F2	F3	F4	F5	TOTAL
0-625	22	8	3	1	0	0	34
626-937	22	10	6	2	2	1	43
938-1250	21	9	1	4	2	0	37
1251-1875	10	10	3	0	0	0	23
1876-2500	3	3	0	0	0	0	6
TOTAL	78	40	13	7	4	1	143

Table 7. Breakdown of tornado occurrences by quadrant of 300-mb jet streak beneath which the tornado occurred and F scale (based on the 114 tornadoes that occurred at ≤1250 km from the jet core at 0000 GMT ±3 hours).

	F SCALE						
	F0	F1	F2	F3	F4	F5	TOTAL
LF	27	12	8	3	4	0	54
LR	2	2	0	0	0	0	4
RF	11	6	0	0	0	0	17
RR	25	7	2	4	0	1	39
TOTAL	65	27	10	7	4	1	114

Table 7 relates the F scale of each tornado that occurred at a distance of 1250 km or less from the jet streak center to the four quadrants of the jet beneath which the tornadoes occurred. The 1250 km cut-off was chosen since 80% of the tornadoes occurred within 1250 km of the center of the jet "max". The quadrants were determined roughly by superimposing a cross-hair onto the center point of the jet streak and noting the location of each tornado. Curvature of the jet streak was not taken into account. The majority

of the tornadoes occurred beneath either the LF (47%) or RR quadrant (34%). A chi-square test shows that there is some statistical association (significant at the .05 level) between jet streak quadrant and tornado intensity. Inspection of the data reveals that there are more F2-F5 tornadoes in the LF quadrant and less F2-F5 tornadoes in the LR and RF quadrants than expected under the assumption of statistical independence. In fact, there were no F2-F5 tornadoes in the LR and RF quadrants.

In conclusion, most of the tornadoes under investigation were F0 or F1 intensity, occurred beneath 15-30 m s^{-1} 300-mb winds, and were located in the LF or RR quadrants of 35-55 m s^{-1} jet streaks at distances of 500 to 1250 km from the center.

3.2 Results of Analysis of the 300-mb Wind Field

Due to limited resources, only nine of the 27 tornado days in May 1977 were selected for quantitative analysis. These nine days (May 4, 5, 15, 16, 17, 18, 19, 20, 21) are of particular interest because of differing types of outbreaks and varying tornado intensities.

Pautz (1969) refined the concept of a tornado outbreak by introducing three outbreak categories: small (6-10 tornadoes), moderate (11-20 tornadoes), and large (>20 tornadoes). Galway (1977) further expanded the outbreak concept by introducing three categories describing the spatial and temporal structure of the outbreak: local (the tornado activity is confined to a roughly circular area of ~10^4 km^2 with a duration of ≤7 hours), progressive (the activity advances generally from west to east covering a distance normally >650 km with a duration of ~9.5 hours), and line (the activity is generally oriented north-south with tornadoes occurring nearly simultaneously at widely separated locations covering an area ~10^5 km^2 with a duration of ~8 hours). In this study, tornado occurrences were categorized as isolated, local outbreak, progressive outbreak, or line outbreak. The outbreak categories were further described as small, moderate, or large.

Table 8 shows the day, number of tornadoes occurring within 3 hours of 0000 GMT, and the type of occurrence. Of all the tornadoes that occurred in the 6-hour interval in May 1977, 74% happened during these 9 days. Thus, the 106 tornadoes are a representative sample of the May 1977 tornado activity.

Values of 300-mb divergence, horizontal wind shear, and positive vorticity advection (PVA) were determined for each tornado. Three hundred-millibar height tendency values at tornado locations were deemed irrelevant since the 0000 GMT 12-hour height changes are centered around 1800 GMT (see 2.2.5 for explanation). Instead, height tendencies upstream from the tornado activity were noted. The presence of an area of significant height falls upstream from the tornadoes is of particular interest since this area might have moved in six hours to correspond spatially with the region of tornado activity. This will be discussed in more detail later in this section. Ten tornadoes were neglected because they fell outside the objective analysis grid, reducing the sample size to 96 tornadoes.

Table 8. Number of tornadoes at 0000 GMT ±3 hours and type of occurrence for each day of interest in May 1977.

DAY	NUMBER OF TORNADOES	TYPE OF OCCURRENCE
4	18	Large Progressive
5	8	Small Progressive
15	4	Isolated
16	13	Isolated
17	9	Small Line
18	18	Large Line
19	9	Isolated
20	16	Large Progressive
21	11	Small Local
TOTAL	106	

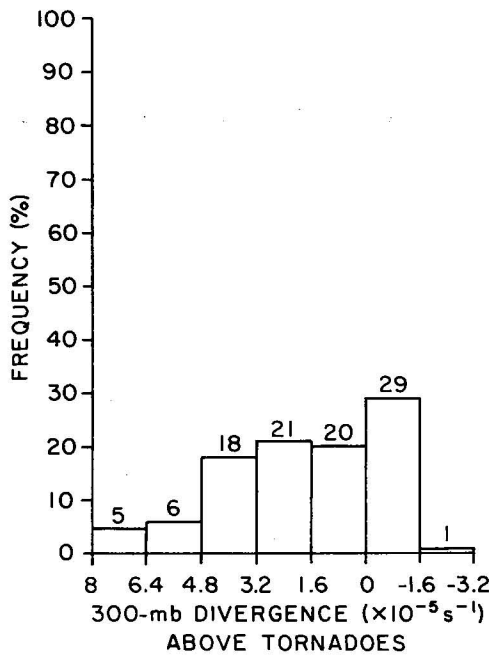

Figure 11. Histogram of 300-mb divergence (x 10^{-5} s^{-1}) for 96 tornadoes that occurred at 0000 GMT ±3 hours (based on data from nine days in May 1977).

Figure 11 is a histogram of divergence values for each tornado. The mean value is 1.8 x 10^{-5} s^{-1} and the standard deviation is 2.3 x 10^{-5} s^{-1}. Sixty-seven of the 96 tornadoes occurred beneath divergent areas. Since 67 is considerably larger than the critical value, 56.1, for the test of the null hypothesis that tornadoes do not occur preferentially beneath upper-level divergence, the apparent bias of tornadoes toward 300-mb divergent flow regions is statistically significant. Forty-one percent of the tornadoes were associated with divergence values between zero and 3.2 x 10^{-5} s^{-1}. Twenty-nine percent occurred in connection with divergence values greater than 3.2 x 10^{-5} s^{-1} and 5% occurred in the range 6.4 to 8.0 x 10^{-5} s^{-1}. Though 30% of the tornadoes happened below convergent areas, most occurred for weak values (zero to -1.6 x 10^{-5} s^{-1}). In contrast, McNulty (1978) found in his study that less than 6% of the tornadoes were associated with strong divergence (average 300-200-mb divergence greater than 2.5 x 10^{-5} s^{-1}). This discrepancy between McNulty's findings and the present ones may be attributed to the differing response functions of the objective analysis schemes used in the two investigations. McNulty's scheme yields lower values of divergence probably because it dampens the shorter waves more. A chi-square test reveals no significant correlation at the 5% level between the intensity (F scale) of a tornado and the divergence at 300-mb.

A histogram of the horizontal shear values for each tornado is shown in Fig. 12. Positive and negative values correspond to cyclonic and anticyclonic shear, respectively. The distribution has a mean of -0.3 x 10^{-5} s^{-1} and a standard deviation of 1.9 x 10^{-5} s^{-1}. The null hypothesis that tornadoes are as likely to occur in cyclonic as in anticyclonic shear areas could not be rejected at the five percent level of significance. The probability of obtaining the observed number of anticyclonic shear tornadoes (54) under the null hypothesis is 0.11.

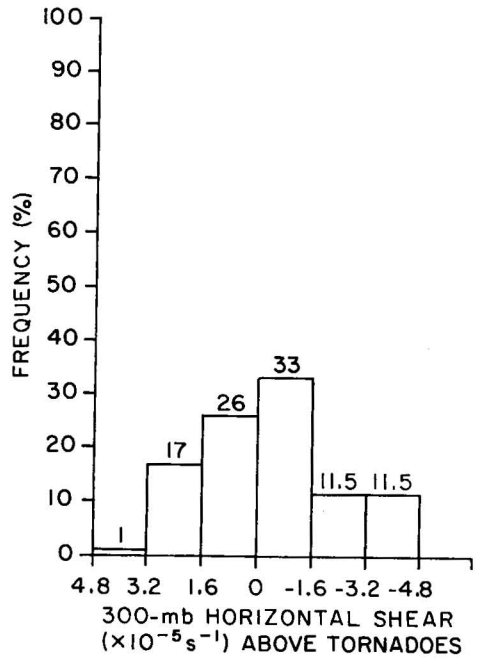

Figure 12. Histogram of 300-mb horizontal wind shear (x 10^{-5} s^{-1}) for 96 tornadoes.

A chi-square test shows there is a relationship between the sign of 300-mb wind shear (cyclonic or anticyclonic) and tornado intensity at the 5% level of significance. Examination of the data reveals a tendency for weak tornadoes (F0) to occur in anticyclonic shear regions and for stronger tornadoes (≥F1) to favor cyclonic shear. This result is completely opposite to Hales' (1979) conclusion but is consistent with our previous finding of more strong tornadoes than expected in the LF quadrant of jet streaks (see Section 3.1). A larger sample is needed to confirm the result obtained above.

The values of 300-mb vorticity advection for each tornado are shown in the histogram in Fig. 13. Seventy-two of the 96 tornadoes occurred beneath areas of PVA. Under the hypothesis that tornadoes are equally likely in NVA and PVA regions, the chances of observing 72 out of 96 tornadoes in PVA areas are less than one in 10^5. The most favored PVA interval ranged from 16 to 32 x 10^{-10} s^{-2} which accounts for nearly one-third of the tornadoes. The mean and standard deviation of the distribution are 19 x 10^{-10} s^{-2} and 21 x 10^{-10} s^{-2}. A chi-square test detects no correlation between vorticity advection and tornado F scale at the five percent level of significance.

In an effort to discover the combination of 300-mb flow features which were most favorable for tornado occurrence, Table 9 was constructed showing the 300-mb conditions at 0000 GMT for each of the 9 days being considered. Thirty-one tornadoes (33%) occurred with divergence, anticyclonic shear, and PVA. Twenty-five tornadoes (26%) occurred with divergence, cyclonic shear, and PVA. The next most frequent situation (13 tornadoes or 14%) had convergence, anticyclonic shear, and PVA. The remaining combinations of conditions accounted for less than 8 tornadoes each.

Since we have failed to establish that horizontal shear is a statistically significant variable in tornado occurrence, we discard it and examine just the relationship between 300-mb divergence, PVA, and tornado occurrence.

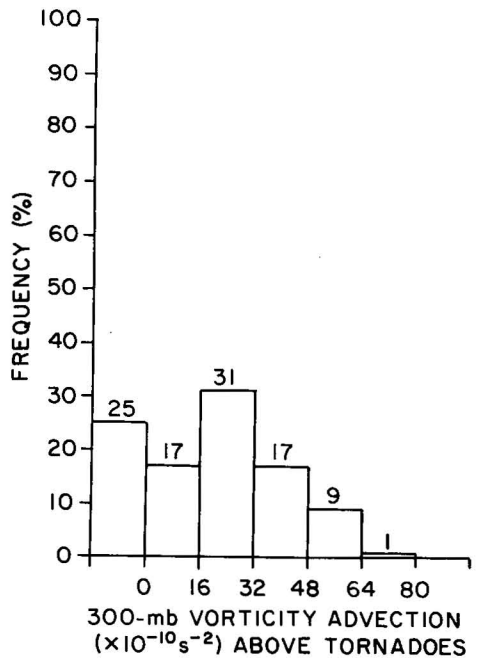

Figure 13. Histogram of 300-mb vorticity advection (x 10^{-10} s^{-2}) for 96 tornadoes.

Table 9. 300-mb conditions at 0000 GMT for each tornado. "Yes" indicates the presence of a parameter and "No" indicates the absence (based on 96 tornadoes).

DAY	NUMBER TORNADOES	DIVERGENCE	ANTICYCLONIC SHEAR	PVA	HEIGHT FALLS UPSTREAM
4 May	4	Yes	Yes	Yes	Yes
	9	Yes	No	Yes	Yes
	2	No	No	No	Yes
	2	No	No	Yes	Yes
5 May	1	No	Yes	No	No
	2	No	Yes	Yes	No
	1	Yes	Yes	Yes	No
	3	Yes	No	Yes	No
15 May	3	Yes	Yes	No	No
16 May	2	No	Yes	Yes	No
	2	Yes	Yes	No	No
	3	No	Yes	No	No
	5	Yes	Yes	Yes	No
	1	No	No	No	No
17 May	1	No	Yes	No	Yes
	6	Yes	No	No	Yes
18 May	2	No	Yes	Yes	Yes
	8	Yes	Yes	Yes	Yes
	5	No	No	No	Yes
19 May	5	Yes	Yes	Yes	No
	3	Yes	No	Yes	No
20 May	1	Yes	Yes	Yes	Yes
	10	Yes	No	Yes	Yes
21 May	2	Yes	Yes	Yes	Yes
	1	No	No	Yes	Yes
	7	No	Yes	Yes	Yes
TOTAL:	96				

Table 10. Chi-square test for independence between 300-mb divergence and vorticity advection (based on 96 tornadoes).

OBSERVED VALUES O_{jk}

	PVA	NVA	TOTAL
Divergence	56	11	67
Convergence	16	13	29
TOTAL	72	24	96

EXPECTED VALUES E_{jk}

	PVA	NVA	TOTAL
Divergence	50.25	16.75	67
Convergence	21.75	7.25	29
TOTAL	72	24	96

$$\chi^2 = \sum \frac{(|O_{jk} - E_{jk}| - 0.5)^2}{E_{jk}} = 7.26 \text{ (using Yates' correction)}$$

$$\chi^2_{1,\ \alpha=.05} = 3.84 \qquad \chi^2_{1,\alpha=.01} = 6.63$$

$\chi^2 > \chi^2_{1,\alpha=.01}$ so null hypothesis can be rejected

Table 10 shows the breakdown of tornadoes that occurred for each of the four possible combinations. Fifty-eight percent of the 96 tornadoes were associated with both divergence and PVA. A chi-square test reveals strong dependence (significant at α = .01 level) between PVA and divergence. This is expected since we have previously shown (Section 1.2) that divergence and PVA are related theoretically.

We return briefly to the subject of 300-mb height tendencies. Since the 0000 GMT height changes are actually centered at 1800 GMT, we look for an area of height falls that lags behind (upstream of) the tornado activity. For this subjective evaluation, the 0000 GMT streamline analysis was used as a guide. For 65 tornadoes, an area of height falls, ranging in intensity

from just less than zero to -120 meters, was indeed located slightly upstream from the activity. Thirty-one tornadoes were associated with height rises upstream, ranging in intensity from 40 to 140 meters. The tornadoes associated with height falls upstream were usually part of an organized outbreak whereas the tornadoes associated with height rises upstream were generally isolated or distributed over a small area.

In review, most of the tornadoes occurred in regions of 300-mb divergence and positive vorticity advection with height fall centers located upstream of the activity. Anticyclonic shear at 300-mb was not found to be a significant parameter. The statistical properties of the variables examined in Sections 3.1 and 3.2 are summarized in Table 11, and the results of tests, which attempted to detect statistical associations between variables are outlined in Table 12.

Note that most of the chi-square tests indicate only that the hypothesis regarding the independence of two variables cannot be rejected at the five percent level of significance with available data. For a larger data set (e.g., several years), the results may be different because the tests will be more powerful. The need for a bigger data collection period arises becauses of the rarity of intense tornadoes. The chi-square tests are not particularly powerful because they do not exploit the quantitative nature of the distinctions between class intervals. More powerful tests, based on regression, might have been able to detect correlations between variables with the present data set. This possibility should be explored.

We should recognize the many sources of error which affect the statistics. Some tornadoes may go unreported while the intensity of others may be misclassified. Flow features may move significant distances between the time they are measured and tornado time. Small-scale disturbances may be inadequately resolved by the upper air network. The measurements themselves are subject to errors, and the grid point values are even more uncertain because they are inferred from the station values by objective analysis.

3.3 Comparison of Two Progressive Tornado Outbreaks

May 1977 was characterized by several tornado outbreaks. Two of these days, 4 May and 20 May, are of particular interest. Both had large progressive outbreaks with several intense tornadoes.

May 4 had 28 tornadoes, 18 of which occurred within 3 hours of 0000 GMT 5 May (see Fig. 14). The 0135 GMT NMC radar summary chart showing storm echo positions near tornado time is presented in Fig. 15. The 300-mb winds at 0000 GMT (Fig. 16) were of moderate strength over the tornado activity. Two wind maxima were in the general vicinity, one (45-55 m s^{-1}) over the Great Salt Lake and the other (35-45 m s^{-1}) over southern Oklahoma. Figure 17, the 0000 GMT 300-mb streamline analysis, shows southwesterly flow with considerable diffluence over the tornado activity. An area of maximum height falls of moderate intensity (80 m) lagged behind (i.e., upstream of) the tornadoes. The 0000 GMT 300-mb divergence and vorticity analyses are shown in Fig. 18. Divergence covered most of the tornado region with a maximum of 4.8 to 6.4 x 10^{-5} s^{-1} over southern Minnesota. However, the tornadoes occurred

Table 11. Statistics of variables examined in Sections 3.1 and 3.2.

VARIABLE	SAMPLE SIZE	MEAN	STANDARD DEVIATION	REMARKS
300-mb wind speed above tornado	143	23.3 m s^{-1}	7.6 m s^{-1}	Test indicates that tornadoes occur below higher than average 300-mb wind speeds
300-mb winds measured at stations	1744	18.5 m s^{-1}	10.0 m s^{-1}	
300-mb wind speed maxima near tornado	143	42.6 m s^{-1}	7.7 m s^{-1}	
Distance of tornado from jet streak	143	937 km	434 km	
Average intensity of tornado	143	F0.8		Only 25 were of F2 or greater intensity
Quadrant of jet streak beneath which tornado occurred	114			54 in left front, 39 in right rear
300-mb divergence above tornado	96	1.8×10^{-5} s^{-1}	2.3×10^{-5} s^{-1}	Mean significantly different from zero
300-mb horizontal wind shear above tornado	96	-0.3×10^{-5} s^{-1}	1.9×10^{-5} s^{-1}	Mean not significantly different from zero
300-mb vorticity advection above tornado	96	19×10^{-10} s^{-2}	21×10^{-10} s^{-2}	Mean significantly different from zero

Table 12. Results of chi-square tests in Sections 3.1 and 3.2.

VARIABLE 1 and Class Invervals Used	VARIABLE 2 and Class Invervals Used	χ^2	(α=.05) χ^2_{crit}	APPARENT STATISTICAL ASSOCIATION
Wind Speed of Jet Core (m s^{-1}) 25-35, 35-45, >45	Distance of Tornado From Jet Core (km) 0-625, 626-1250, >1250	5.69	9.49	No
Tornado Intensity (F Scale) F0, F1, ≥F2	Overlying 300-mb Wind Speed (m s^{-1}) ≤25, >25	1.45	5.99	No
Tornado Intensity (F Scale) F0, F1, ≥F2	Wind Speed of Jet Core (m s^{-1}) 25-35, 35-45, >45	7.85	9.49	No
Tornado Intensity (F Scale) F0, F1, ≥F2	Distance of Tornado From Jet Core (km) 0-625, 626-1250, >1250	7.48	9.49	No
Tornado Intensity (F Scale) F0, F1, ≥F2	Quadrant of Jet Streak LF,RR; RF,LR	7.32	5.99	Yes
Tornado Intensity (F Scale) F0, F1, ≥F2	300-mb Divergence ($x10^{-5}$ s^{-1}) >3.2, 3.2-0, <0	6.37	9.49	No
Tornado Intensity (F Scale) F0, F1, ≥F2	300-mb Horizontal Wind Shear ($x10^{-5}$ s^{-1}) >0, <0	7.27	5.99	Yes
Tornado Intensity (F Scale) F0, F1, ≥F2	300-mb Vorticity Advection ($x10^{-10}$ s^{-2}) <16, 16-32, >32	3.69	9.49	No
300-mb Vorticity Advection ($x10^{-10}s^{-2}$) >0, <0	300-mb Divergence ($x10^{-5}$ s^{-1}) >0, <0	7.26	6.63*	Yes

* α = .01

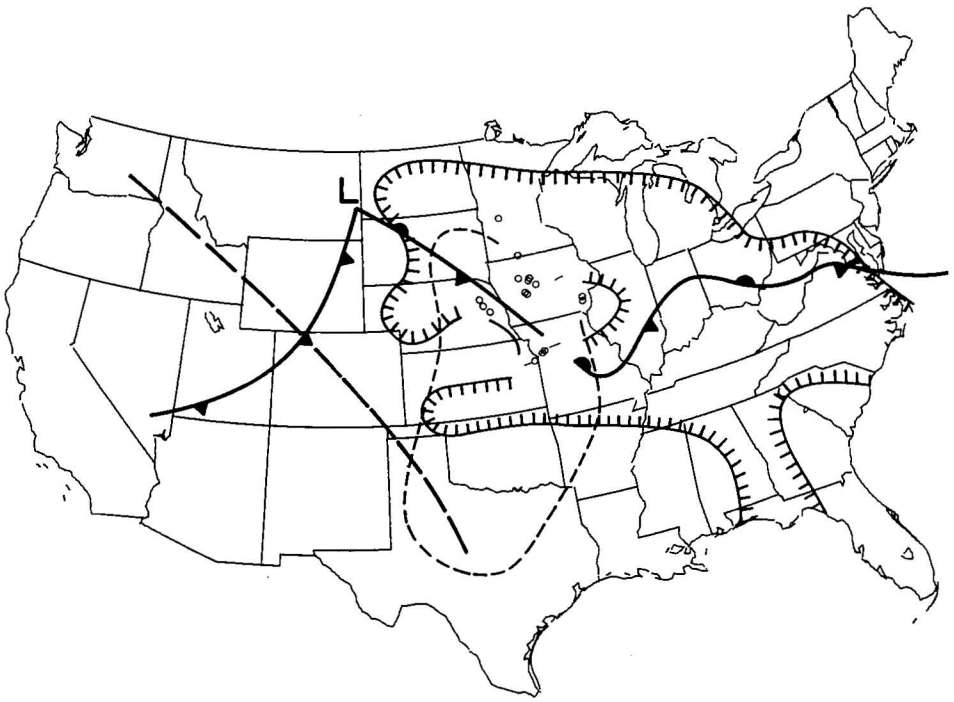

Figure 14. Composite map for 4 May 1977 with 1200 GMT surface fronts, 850-mb moisture (hatched edging) and low-level jet (thin dashed line, generally ≥30 knots), 500-mb shortwave trough (thick dashed line), and 18 tornadoes at 0000 GMT ±3 hours. Circle indicates tornado with path length <15 miles. Line is proportional to path length ≥15 miles.

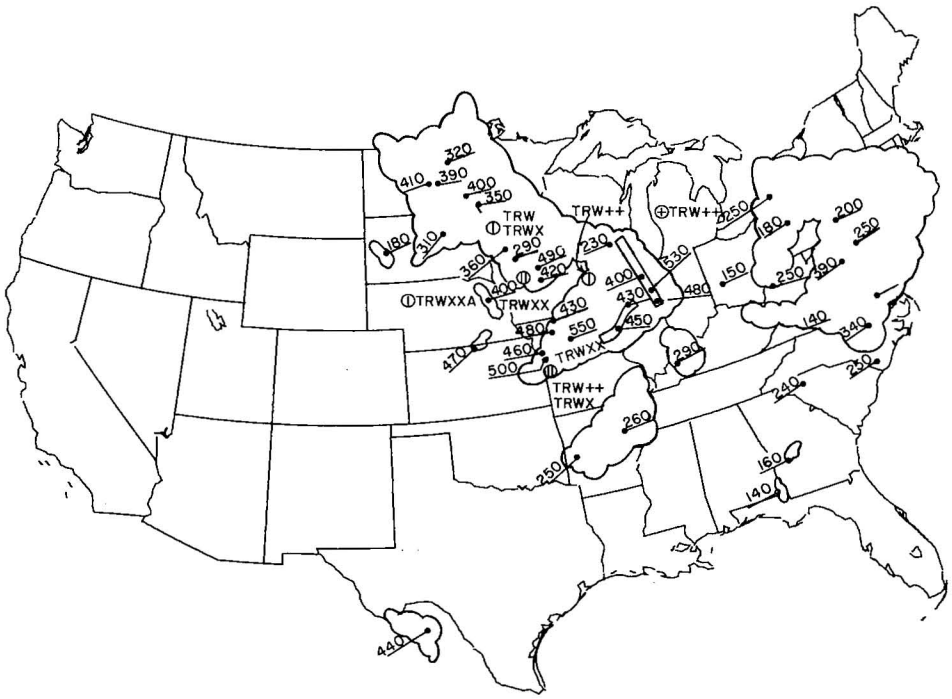

Figure 15. NMC radar summary chart for 0135 GMT 5 May 1977.

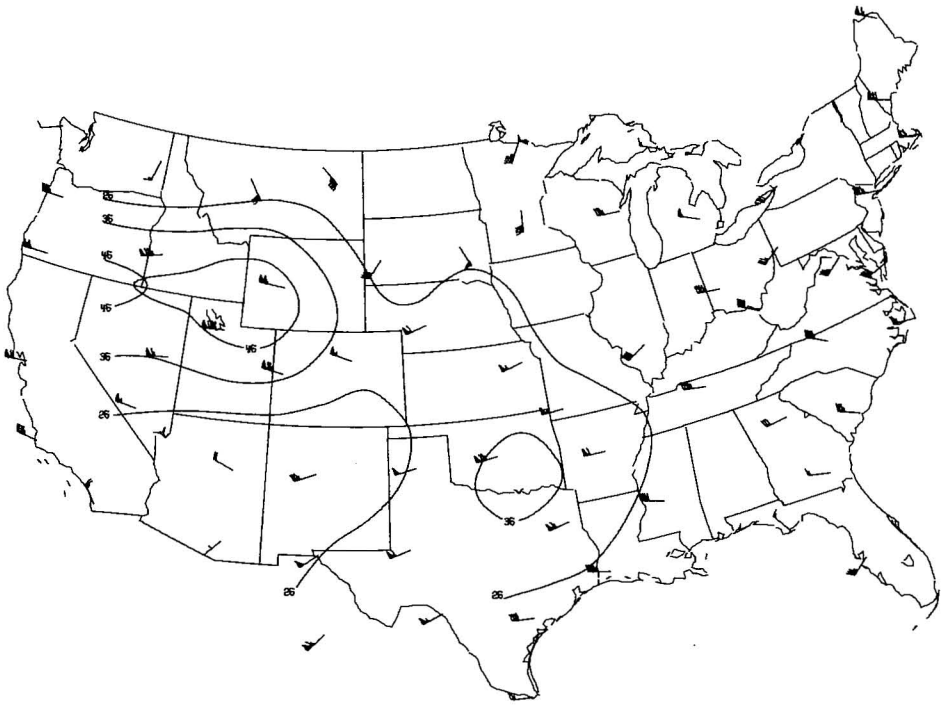

Figure 16. 300-mb isotach analysis (m s^{-1}) for 0000 GMT 5 May 1977. Each full barb is 5 m s^{-1}, half barb is 2.5 m s^{-1}, and flag is 25 m s^{-1}.

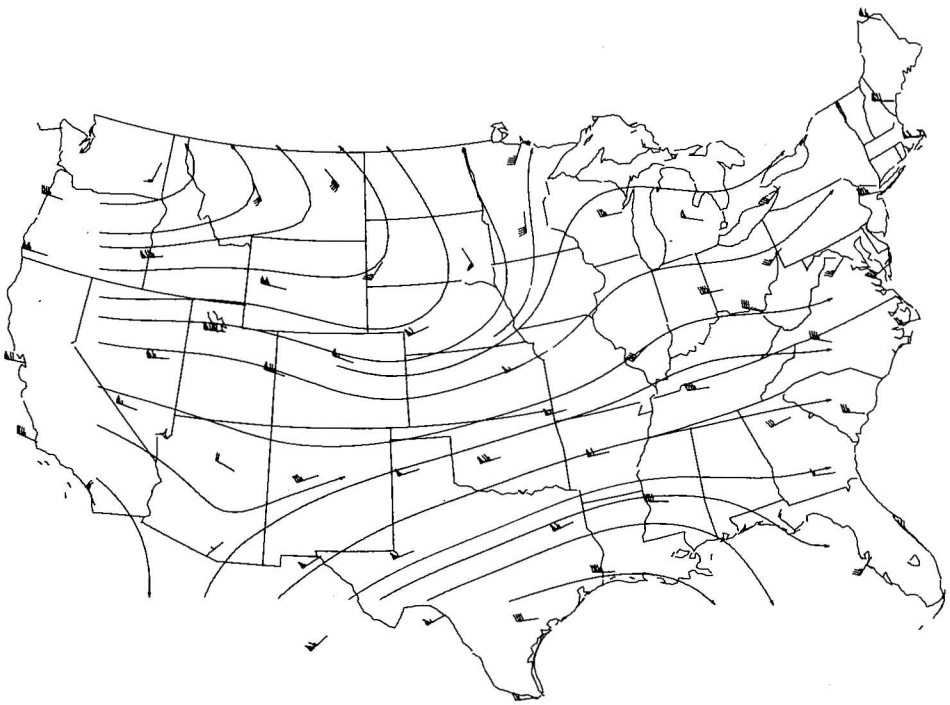

Figure 17. 300-mb streamline analysis for 0000 GMT 5 May 1977.

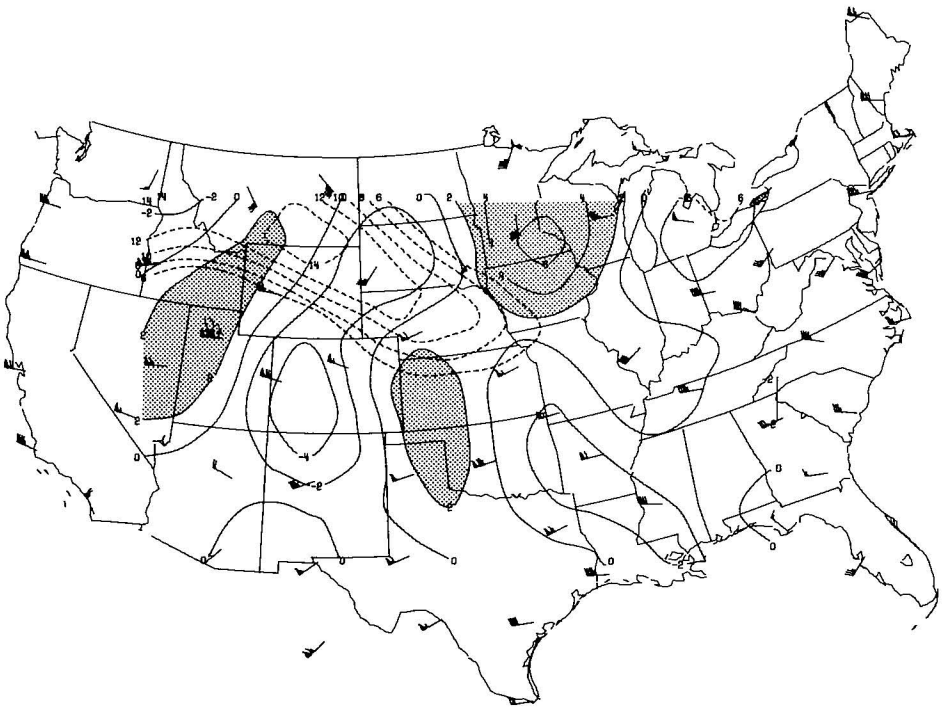

Figure 18. 300-mb divergence (x 0.8 x 10^{-5} s^{-1}, solid lines) and relative vorticity (x 0.8 x 10^{-5} s^{-1}, dashed lines) analysis for 0000 GMT 5 May 1977 (shading indicates divergence $\geq$1.6 x 10^{-5} s^{-1}). Contours of relative vorticity are drawn only for values $\geq$4.8 x 10^{-5} s^{-1}.

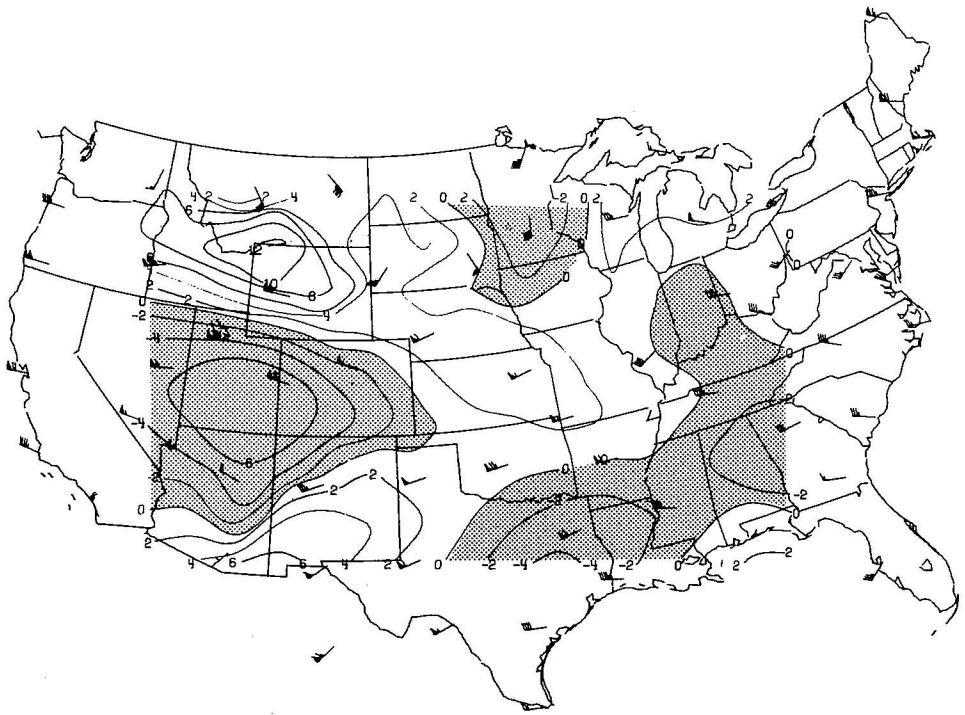

Figure 19. 300-mb horizontal wind shear analysis (x 0.8 x 10^{-5} s^{-1}) for 0000 GMT 5 May 1977. Shading indicates anticyclonic shear.

beneath the divergence gradient, not beneath the maximum. A relative vorticity ridge was brushing the northern edge of the activity, but most of the tornadoes occurred beneath rather weak relative vorticity (<4.8 x 10^{-5} s^{-1}). The 0000 GMT 300-mb horizontal wind shear (Fig. 19) was generally weak (±1.6 x 10^{-5} s^{-1}) in the vicinity of the tornadoes. A band of PVA (Fig. 20) stretched across the entire tornado area at 0000 GMT with a maximum of 32 to 48 x 10^{-10} s^{-2} centered over southeastern Iowa and western Illinois.

May 20 had 24 tornadoes, 16 of which occurred within 3 hours of 0000 GMT 21 May (Fig. 21). The 0135 GMT NMC radar chart is shown in Fig. 22. On this day, the 0000 GMT 300-mb winds (Fig. 23) were slightly stronger over the tornado area and the jet maximum was closer to the activity than on 4 May. There was southwesterly flow with marked streamline diffluence over the region (Fig. 24) as on 4 May. An area of maximum height falls (60 m) lagged behind the tornado activity. The 300-mb divergence at 0000 GMT (Fig. 25) was much greater than on 4 May with a maximum of 6.4 to 8.0 x 10^{-5} s^{-1} over extreme southwestern Oklahoma. All of the tornadoes occurred beneath the gradient just ahead of the divergence maximum. Figure 26 shows the contrast in divergence values between 4 May and 20 May. The divergence was much greater over the outbreak on the twentieth. A strong relative vorticity maximum was approaching Oklahoma from the west (Fig. 25) but most of the tornadoes occurred beneath much weaker relative vorticity (<4.8 x 10^{-5} s^{-1}). The 0000 GMT 300-mb horizontal wind shear (Fig. 27) over the outbreak region was roughly the same order of magnitude (±1.6 x 10^{-5} s^{-1}) on 20 May as on 4 May. The most striking difference between the two days was in the amount of PVA present. Figure 28 shows very strong 300-mb PVA over the tornado area at 0000 GMT with a maximum of 80 to 96 x 10^{-10} s^{-2} over southwestern Kansas.

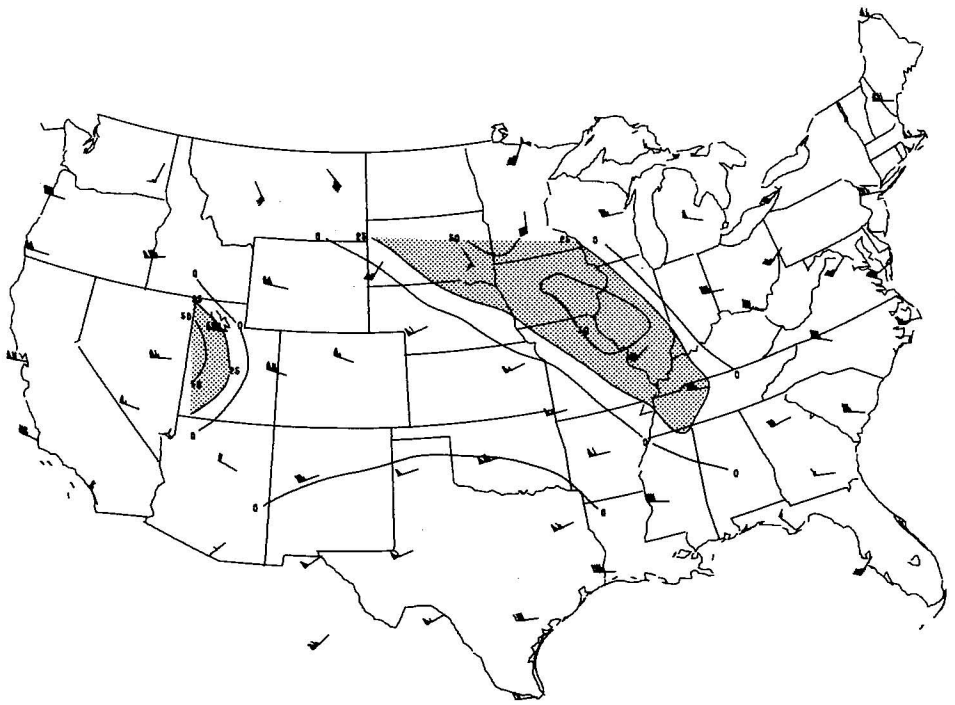

Figure 20. 300-mb positive vorticity advection analysis (x 0.64 x 10^{-10} s^{-2}) for 0000 GMT 5 May 1977. Shading indicates PVA values ≥16 x 10^{-10} s^{-2}.

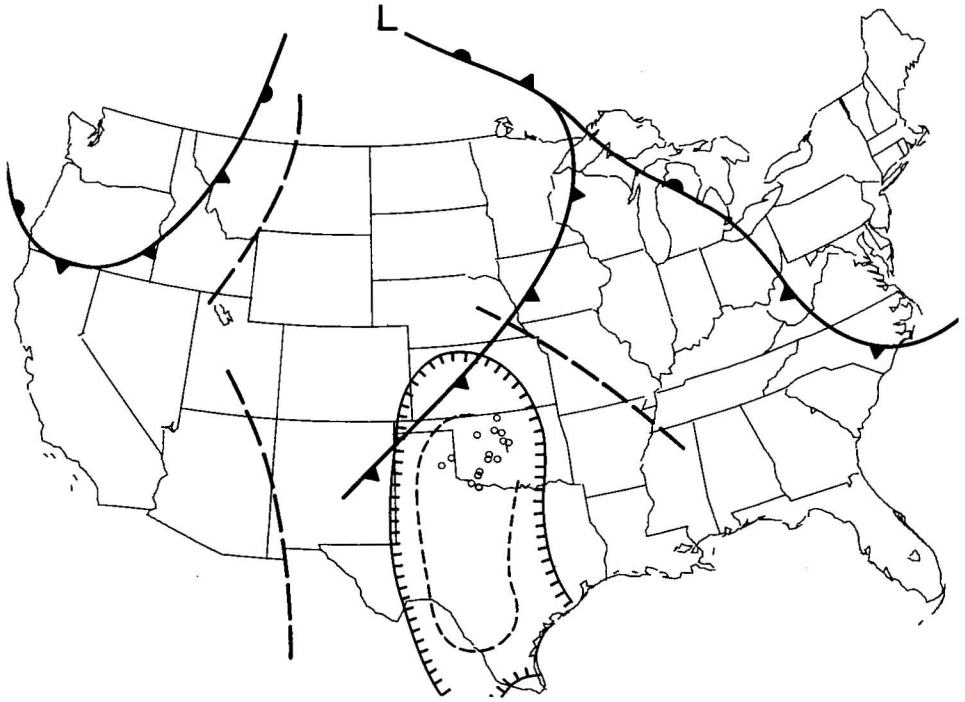

Figure 21. 1200 GMT composite map for 20 May 1977 with 16 tornadoes at 0000 GMT ±3 hours (same as Fig. 13).

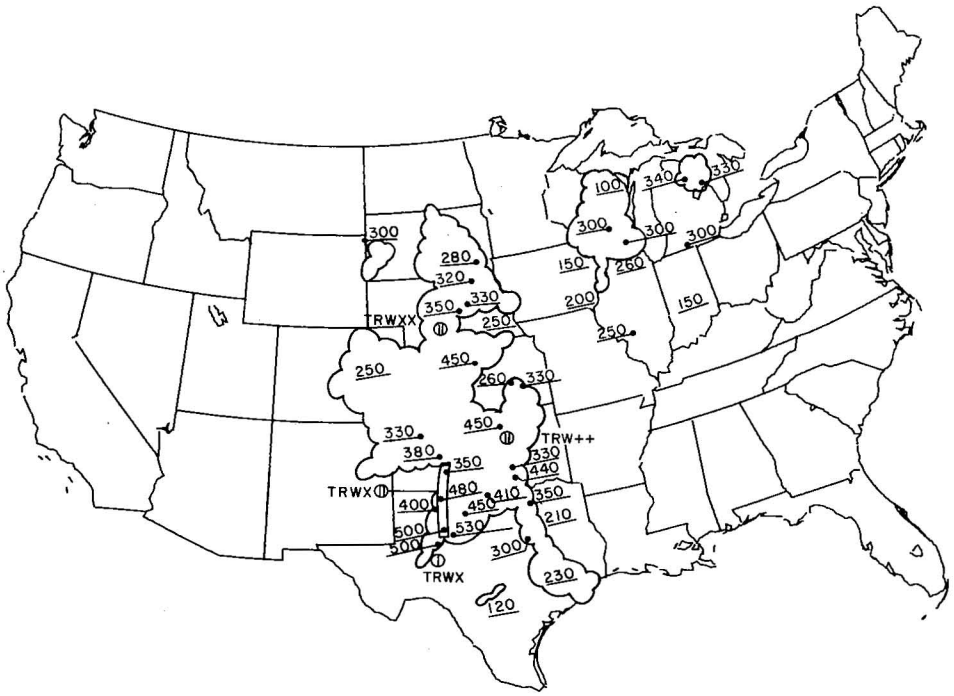

Figure 22. NMC radar summary chart for 0135 GMT 21 May 1977.

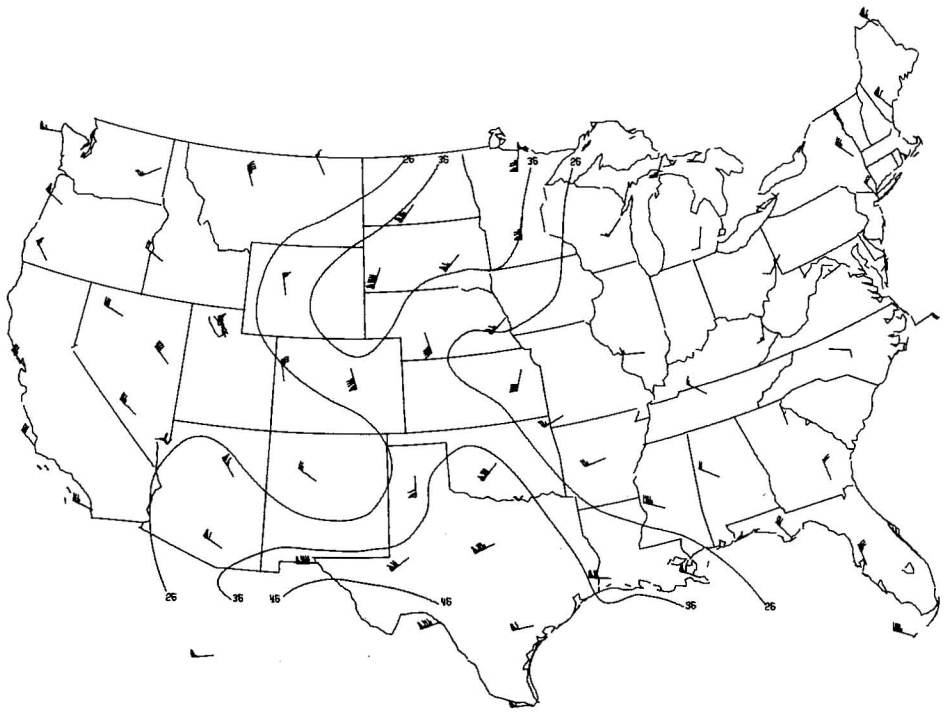

Figure 23. 300-mb isotach analysis for 0000 GMT 21 May 1977 (same as Fig. 15).

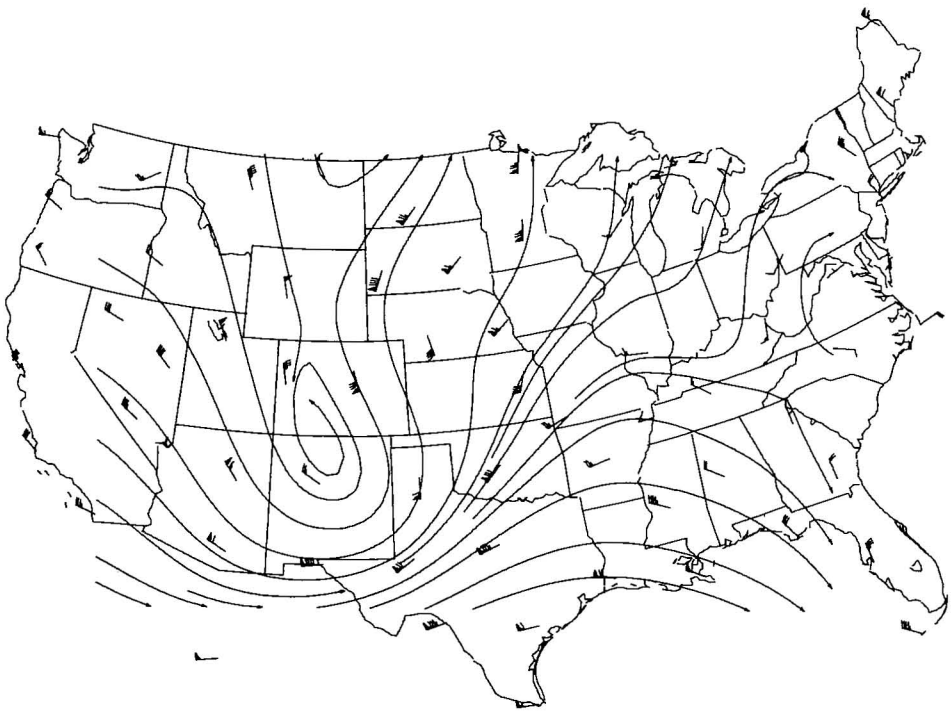

Figure 24. 300-mb streamline analysis for 0000 GMT 21 May 1977.

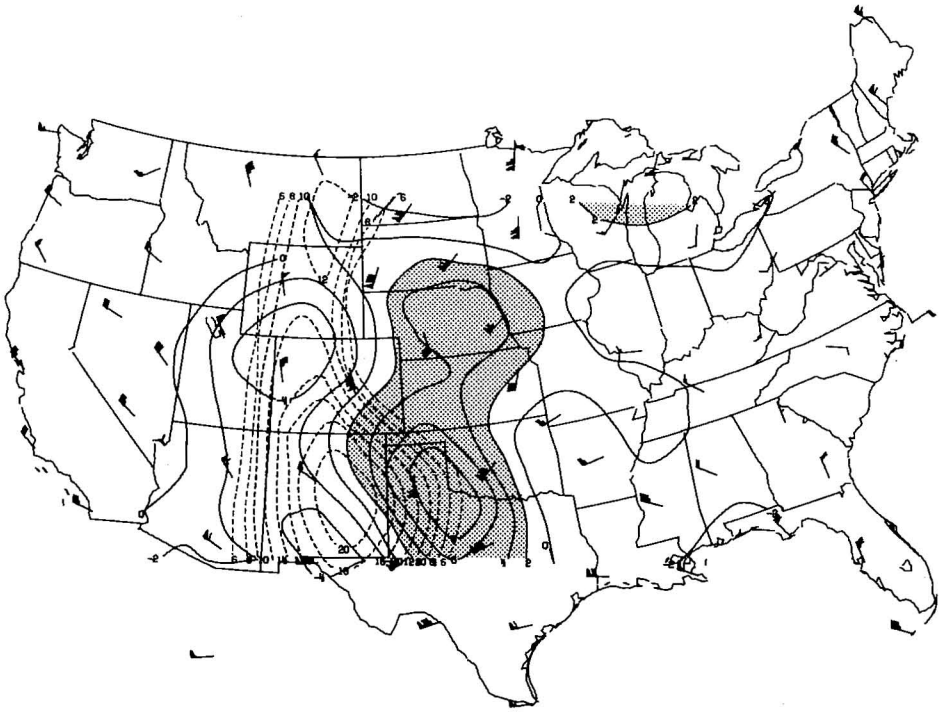

Figure 25. 300-mb divergence and relative vorticity analysis for 0000 GMT 21 May 1977 (same as Fig. 17).

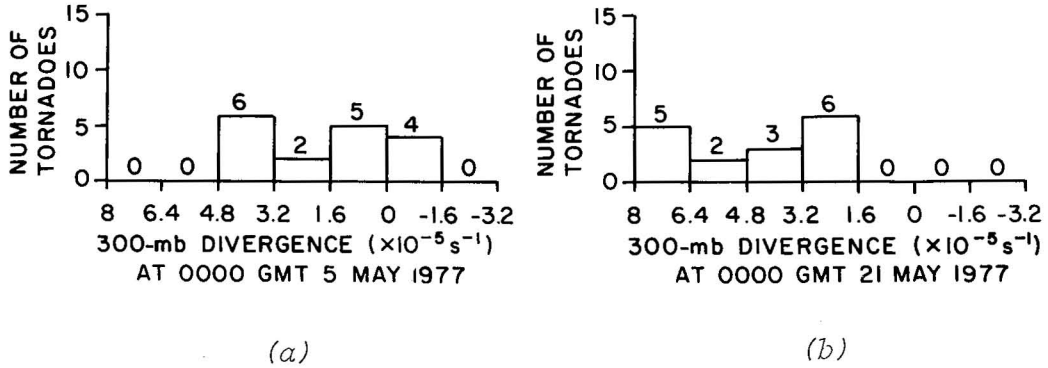

Figure 26. Comparison of 300-mb divergence values above tornadoes for (a) 4 May and (b) 20 May.

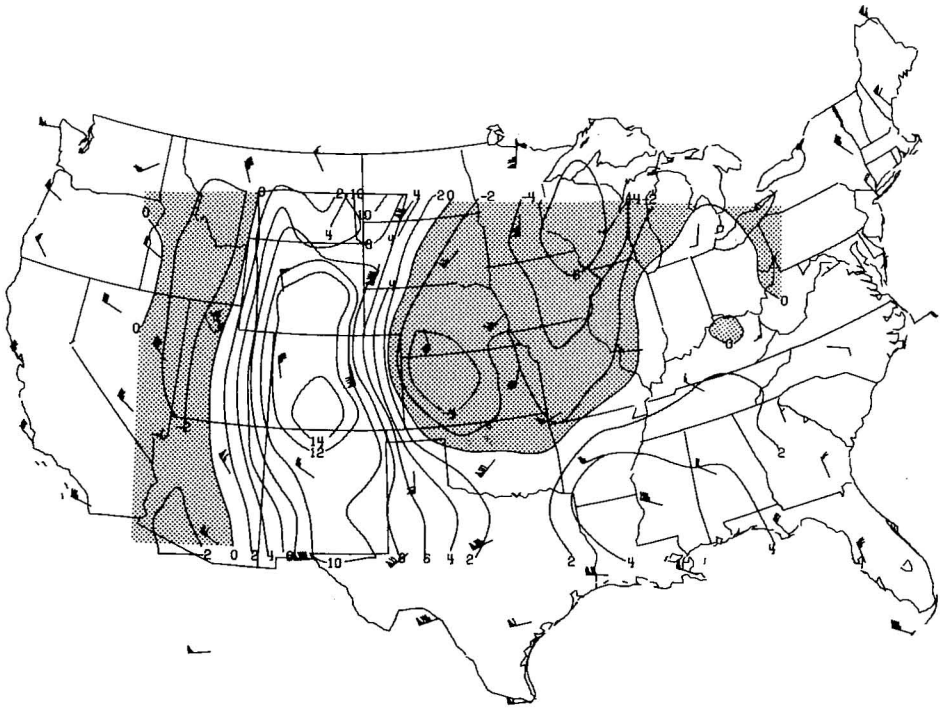

Figure 27. 300-mb horizontal wind shear analysis for 0000 GMT 21 May 1977 (same as Fig. 18).

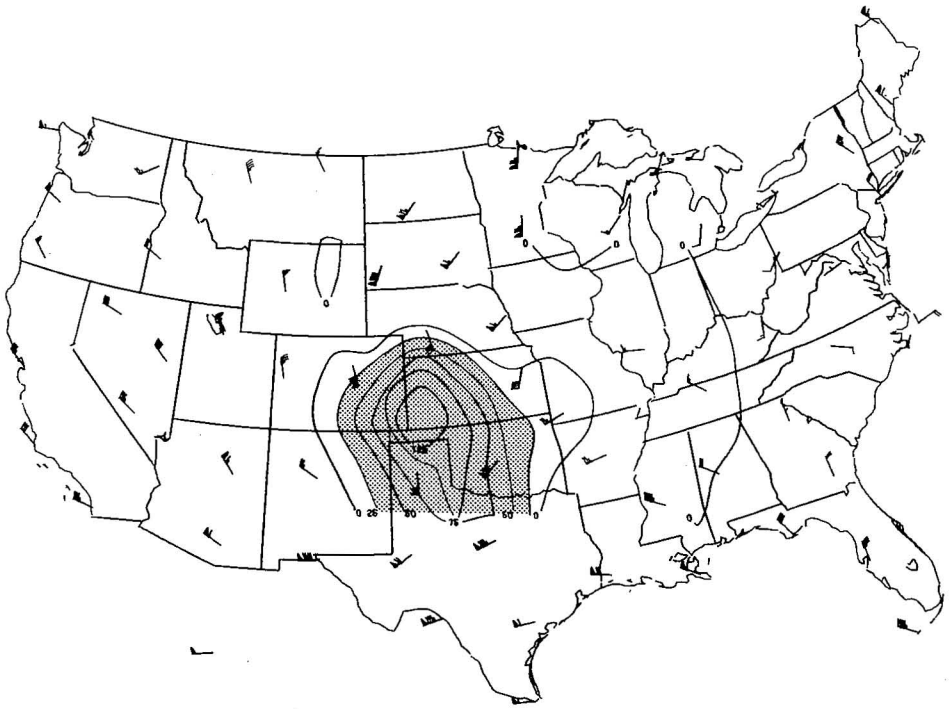

Figure 28. 300-mb positive vorticity advection analysis for 0000 GMT 21 May 1977 (same as Fig. 19).

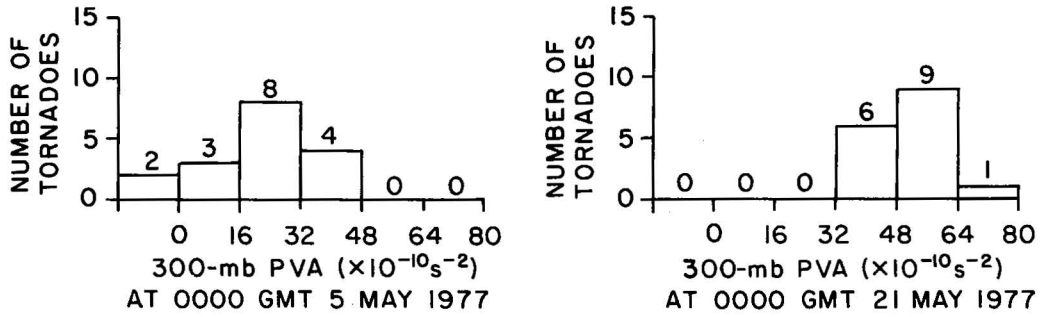

Figure 29. Comparison of 300-mb PVA values above tornadoes for (a) 4 May and (b) 20 May.

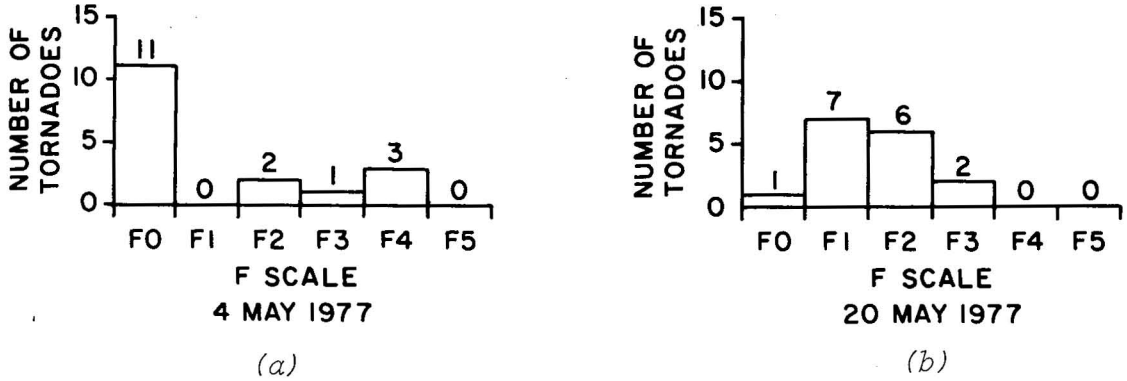

Figure 30. Histogram of tornado F scales for (a) 4 May and (b) 20 May.

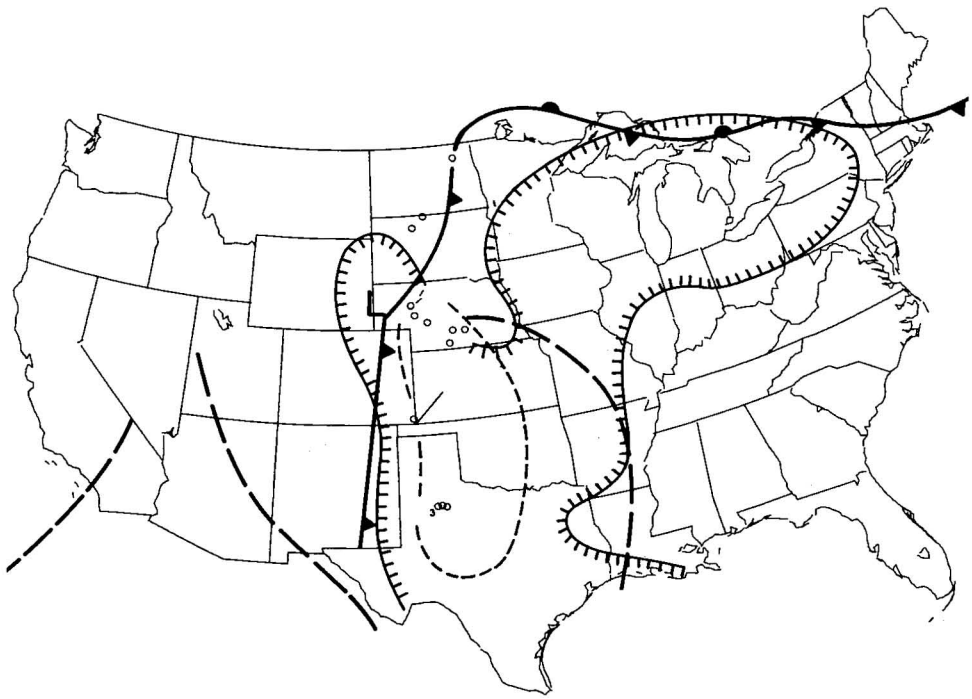

Figure 31. 1200 GMT composite map for 18 May 1977 with 18 tornadoes at 0000 GMT ±3 hours (same as Fig. 13).

All tornadoes occurred beneath the gradient on the leading edge of the PVA ridge. Figure 29 compares the PVA values for the two days. The 20 May values of 300-mb PVA were the strongest encountered in this investigation.

Figure 30 shows the distribution of tornado F scales for each day. While 4 May had several strong tornadoes, most were weak. May 20 had mostly moderate tornadoes, no strong ones, and few weak ones. On the average, the tornadoes were more intense on 20 May, perhaps due to the greater divergence and PVA over the outbreak area.

3.4 Large Line Outbreak of 18 May 1977

On 18 May, a large line outbreak covered the central United States from North Dakota to central Texas. A total of 25 tornadoes were confirmed, 18 of which occurred at 0000 GMT ±3 hours on 19 May (Fig. 31). Figure 32 is the 0135 GMT NMC radar summary chart.

Two strong wind maxima dominated the 0000 GMT 300-mb wind field (Fig. 33). One wind "max" (45-55 m s^{-1}) was centered over northeastern Wyoming while the other (35-45 m s^{-1}) stretched across the Arizona-New Mexico border into southwestern Colorado. Note that the 300-mb jet stream flowed parallel and to the left of the north-south oriented tornado activity. The flow at 300 mb was generally south to southwesterly. Widespread diffluence over the central United States is indicated by the 0000 GMT streamline analysis in Fig. 34. The 0000 GMT height tendency field was relatively flat.

The divergence field (Fig. 35) had a maximum of 4.8 to 6.4 x 10^{-5} s^{-1} centered over western Nebraska, which coincided well with the storm complex shown in Fig. 32. The maximum also coincided with the RR quadrant of the jet streak (Fig. 33) where one might find a divergence maximum. Most of the tornadoes occurred near the divergence maximum. The 300-mb relative vorticity maximum lay well to the west of the tornado activity; hence, all tornadoes occurred beneath weak relative vorticity (<4.8 x 10^{-5} s^{-1}).

The entire central United States was covered by anticyclonic wind shear at 0000 GMT (Fig. 36) with a maximum of 3.2 x 10^{-5} s^{-1} centered over the South Dakota-Nebraska border.

Figure 37 shows the 0000 GMT 300-mb PVA analysis. The maximum in Nebraska coincides well with a cluster of six tornadoes (see Fig. 31). Reports from three stations, Dodge City, Oklahoma City, and Stephenville, were missing and caused a data void from central Texas to western Kansas. These missing observations may account for the apparent weakening or flatness of some of the analyzed fields over the south central United States.

Most of the tornadoes that occurred at 0000 GMT ±3 hours on 19 May were weak (Fig. 38). There was one F5 tornado in Colorado. The long-track tornado in Kansas (128 mi) is a bit misleading. It may actually have been several tornadoes and may have been stronger than F2 but happened mostly over open country where damage and intensity are difficult to estimate.

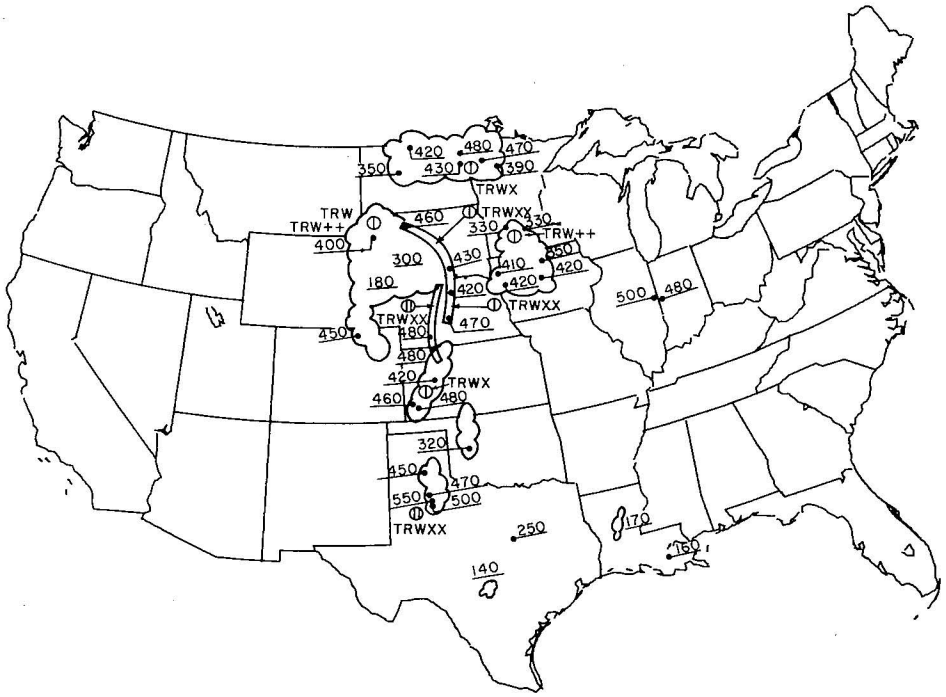

Figure 32. NMC radar summary chart for 0135 GMT 19 May 1977.

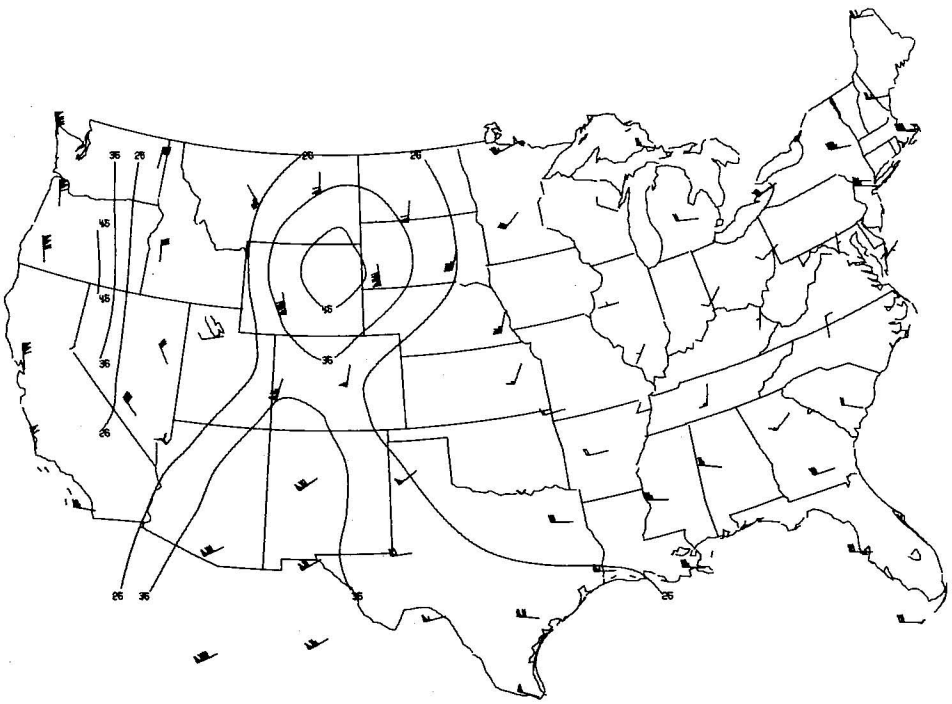

Figure 33. 300-mb isotach analysis for 0000 GMT 19 May 1977 (same as Fig. 15).

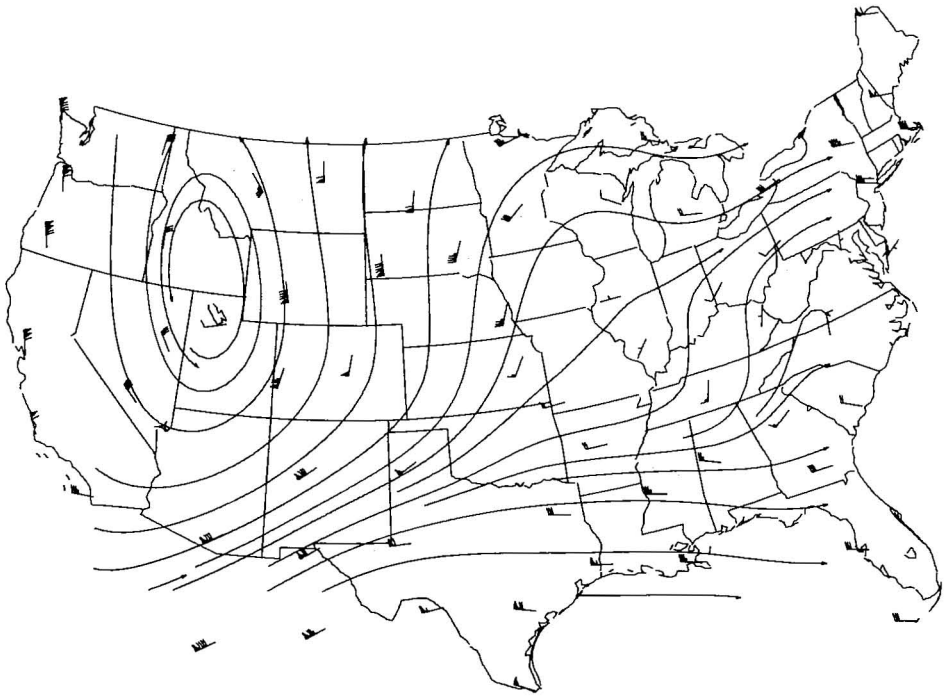

Figure 34. 300-mb streamline analysis for 0000 GMT 19 May 1977.

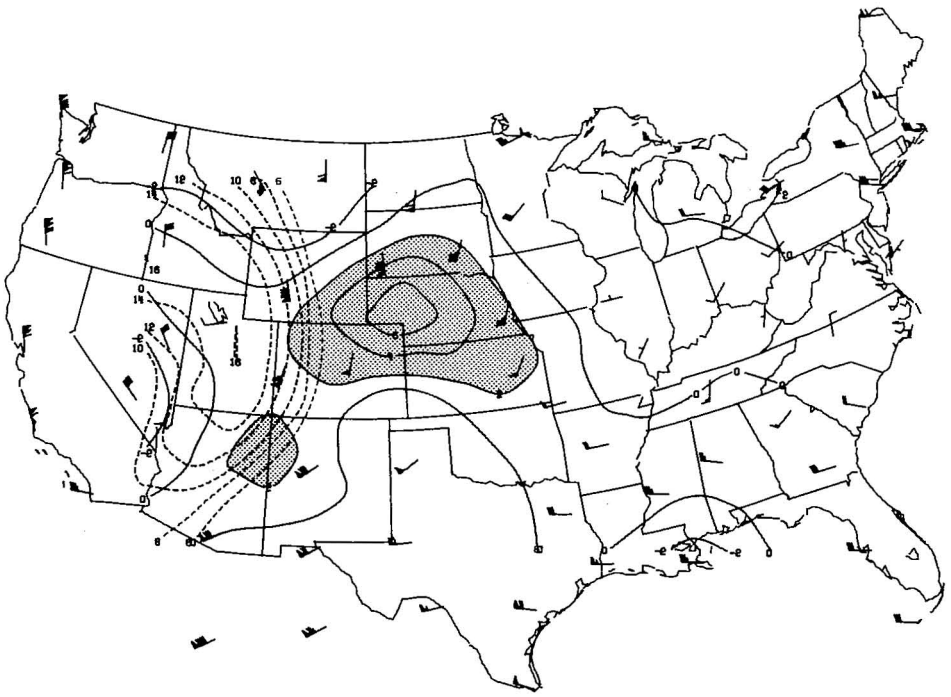

Figure 35. 300-mb divergence and relative vorticity analysis for 0000 GMT 19 May 1977 (same as Fig. 17).

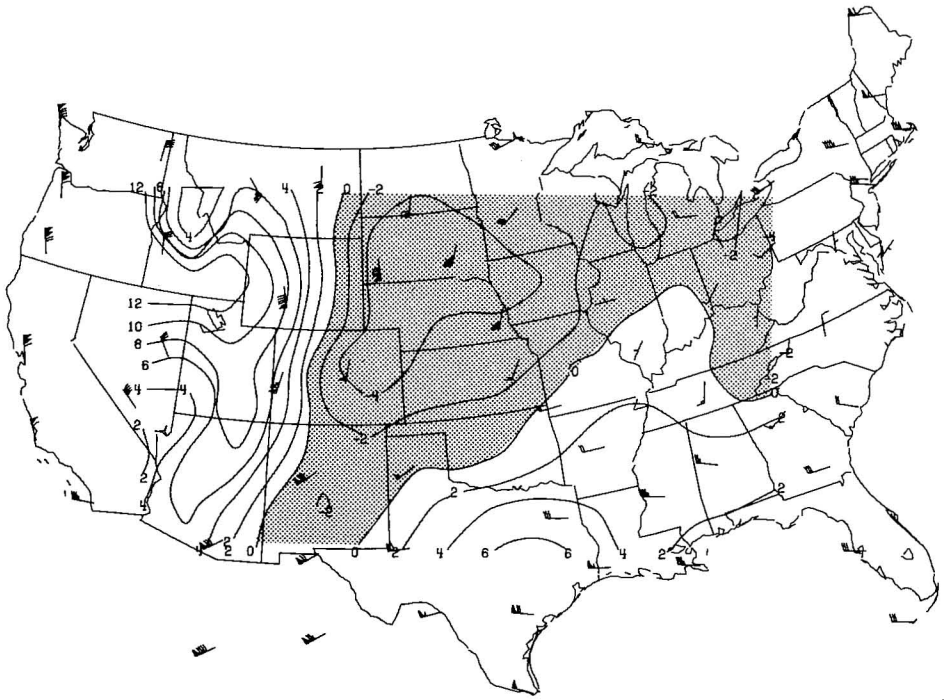

Figure 36. 300-mb horizontal wind shear analysis for 0000 GMT 19 May 1977 (same as Fig. 18).

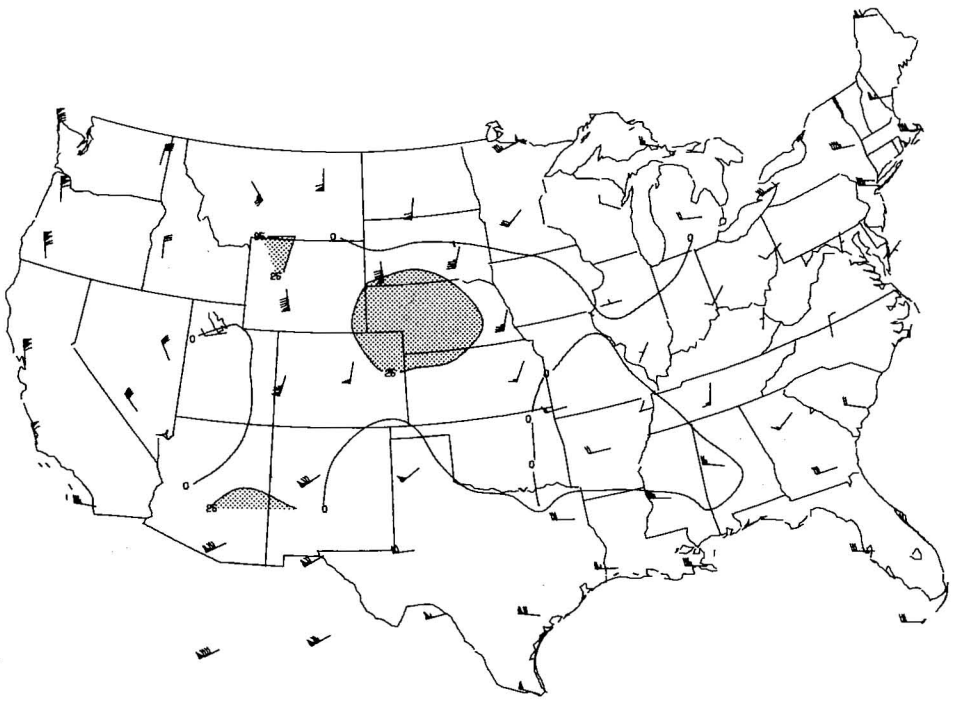

Figure 37. 300-mb positive vorticity advection analysis for 0000 GMT 19 May 1977 (same as Fig. 19).

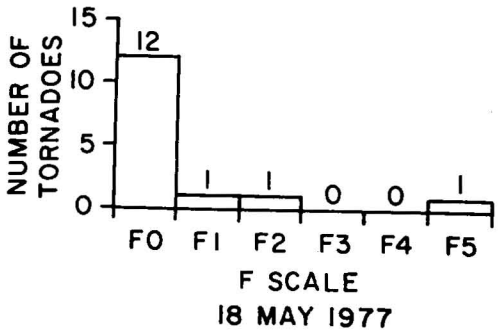

Figure 38. Histogram of tornado F scale for 18 May 1977.

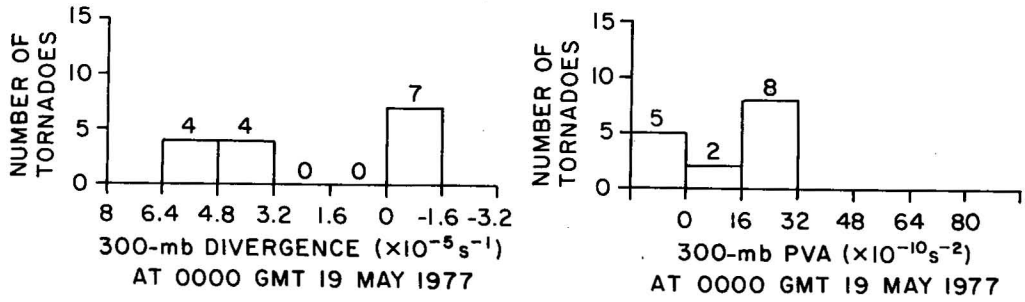

(a) *(b)*

Figure 39. Distribution of 300-mb (a) divergence and (b) PVA values above tornadoes for 0000 GMT 19 May 1977.

The distributions of 300-mb divergence values and PVA values for 18 May are shown in Fig. 39. When these are compared with the corresponding distributions for 20 May (Figs. 26,29), it becomes evident that the 300-mb dynamics were not as strong on 18 May. Perhaps, this accounts to some extent for the predominance of weak tornadoes.

3.5 Isolated Tornadoes of 16 May 1977

The case of 16 May 1977 provides an interesting contrast to the three days mentioned above. Thirteen tornadoes were confirmed on this day, all occurring at 0000 GMT ±3 hours, but the activity was widely scattered over six states (Fig. 40). Though several squall lines are apparent on the 0135 GMT radar summary chart (Fig. 41), the tornado activity was not an organized outbreak.

The 300-mb winds were of moderate strength (10-25 m s^{-1}) with a small maximum (25-35 m s^{-1}) over Nebraska (Fig. 42). The flow was southwesterly and generally diffluent over the entire central United States with the greatest diffluence over Oklahoma and Kansas (Fig. 43).

At 0000 GMT, most of the central United States was covered by moderate height rises with a maximum of 100 to 120 m centered upstream over Arizona. The divergence field had a maximum of 3.2 to 4.8 x 10^{-5} s^{-1} centered over northwestern Oklahoma (Fig. 44). This corresponds well with the location of

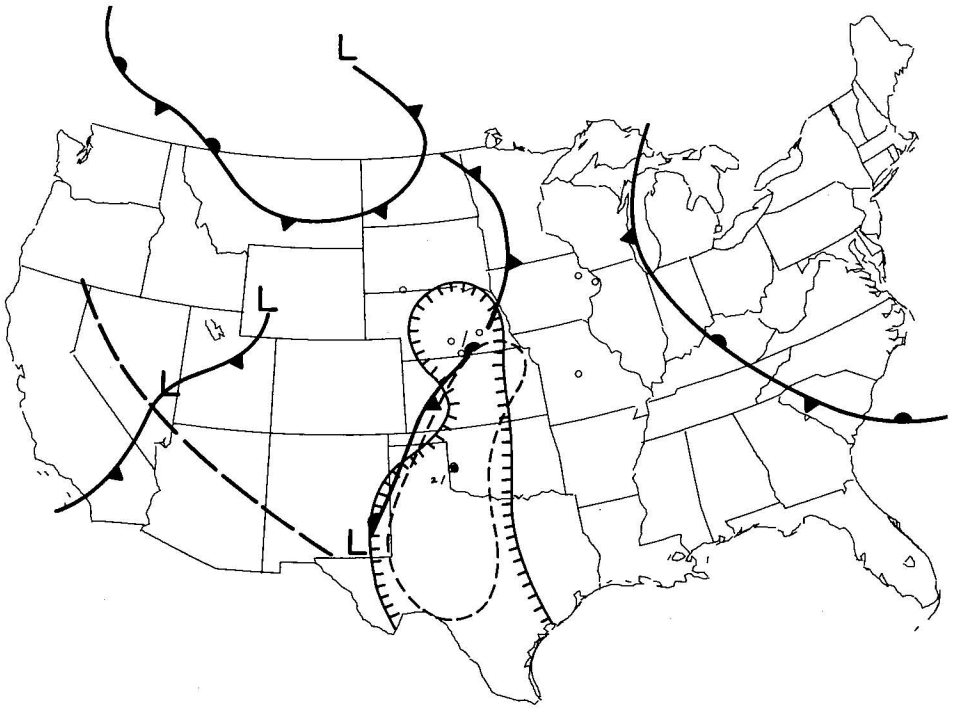

Figure 40. 1200 GMT composite map for 16 May 1977 with 13 tornadoes at 0000 GMT ±3 hours (same as Fig. 13).

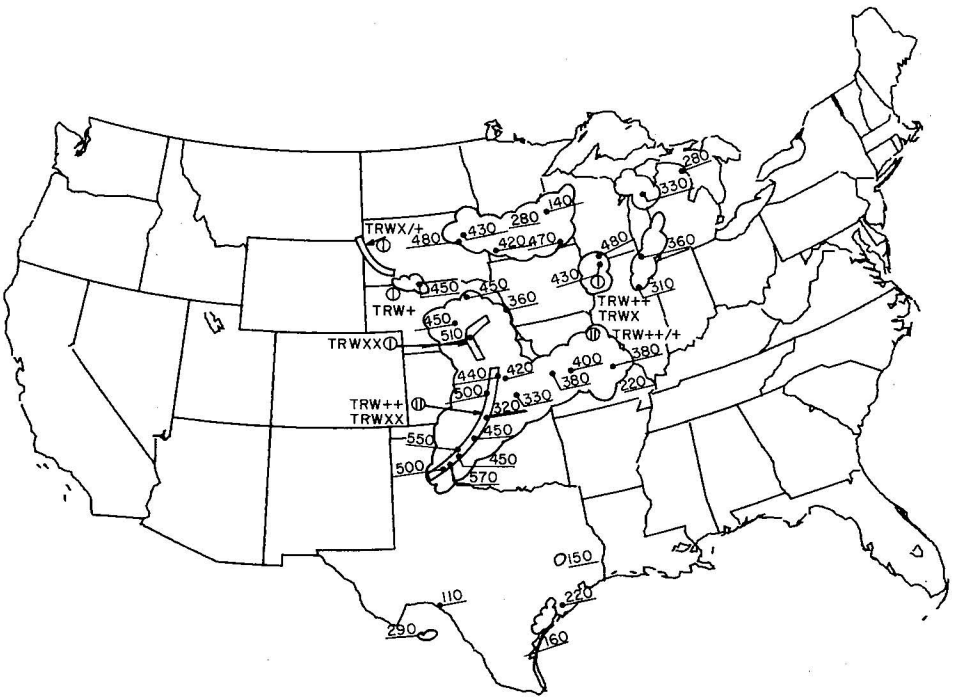

Figure 41. NMC radar summary chart for 0135 GMT 17 May 1977.

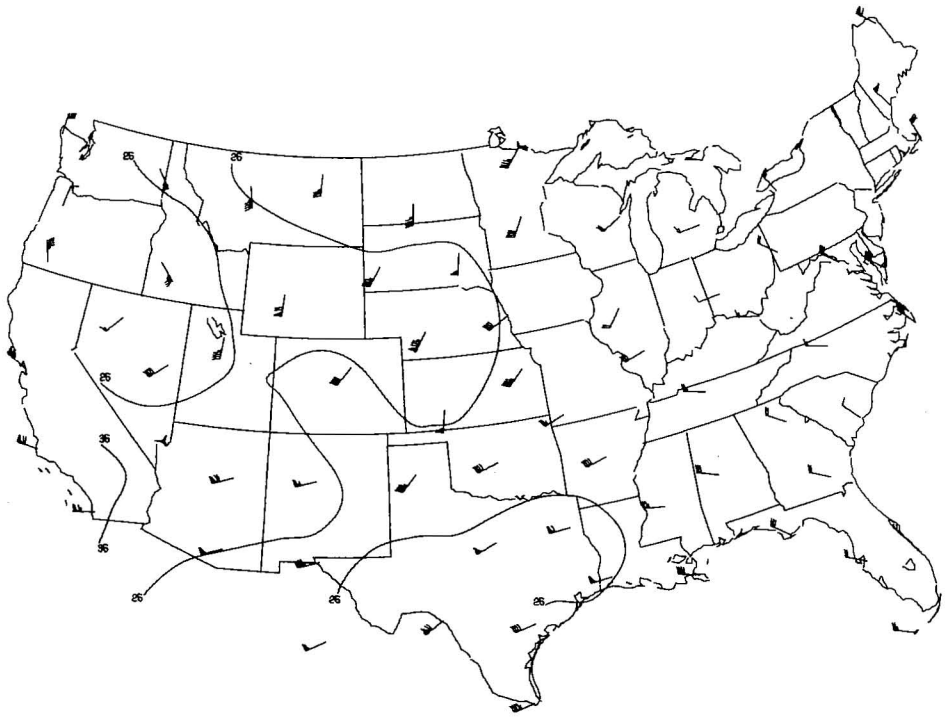

Figure 42. 300-mb isotach analysis for 0000 GMT 17 May 1977 (same as Fig. 15).

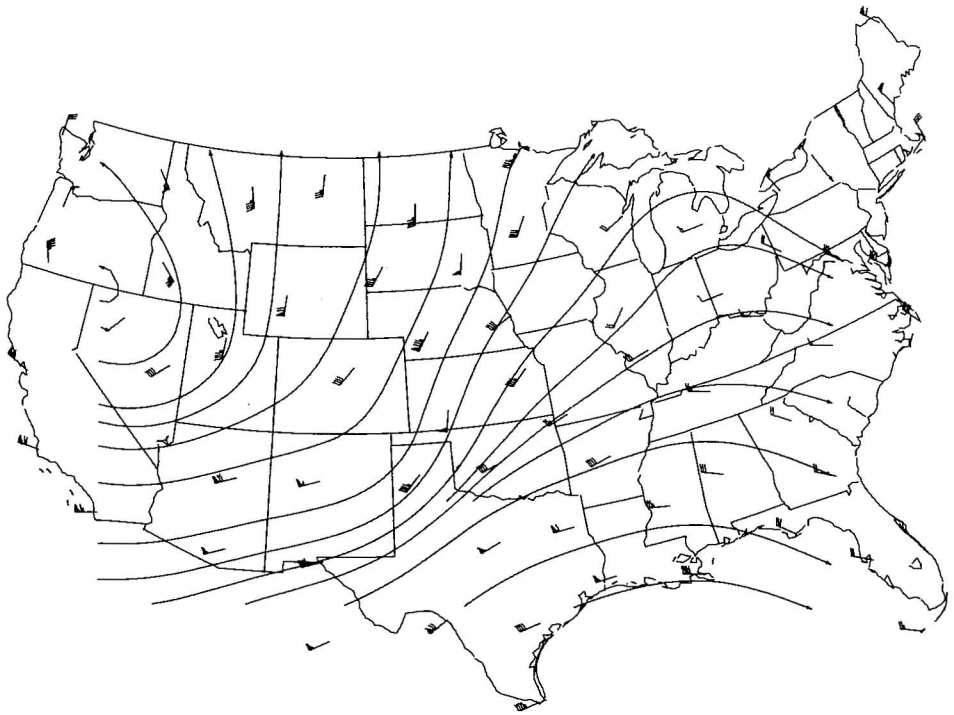

Figure 43. 300-mb streamline analysis for 0000 GMT 17 May 1977.

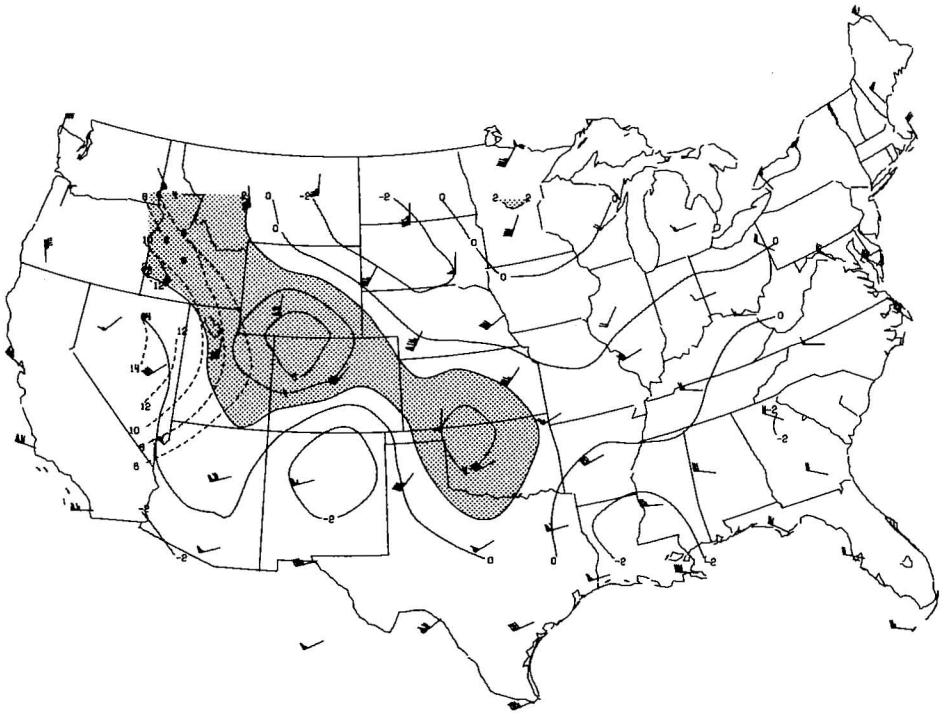

Figure 44. 300-mb divergence and relative vorticity analysis for 0000 GMT 17 May 1977 (same as Fig. 17).

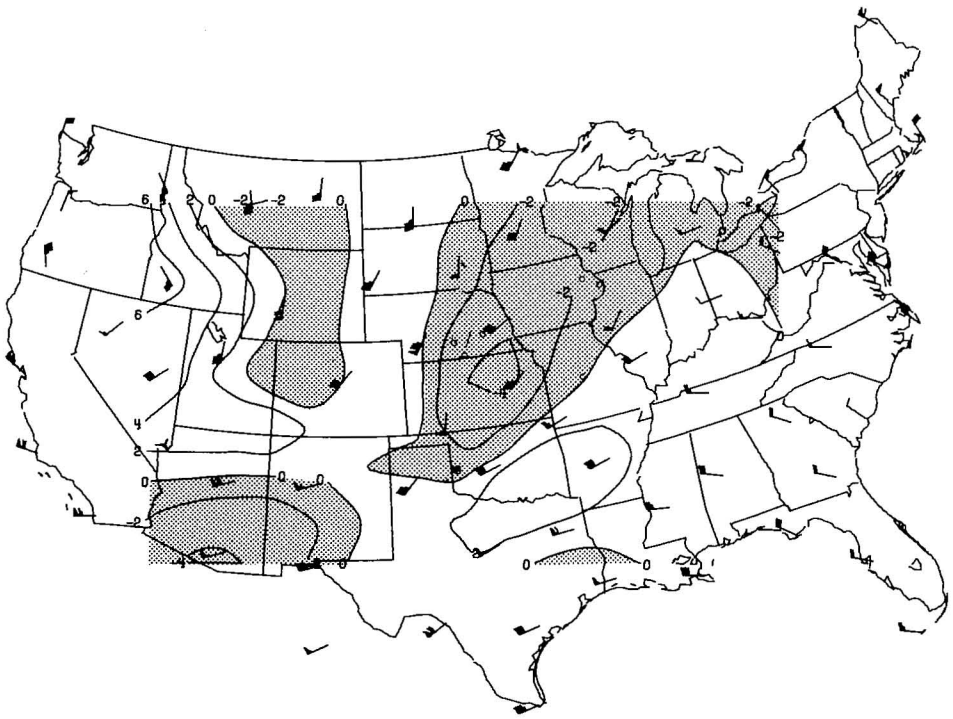

Figure 45. 300-mb horizontal wind shear analysis for 0000 GMT 17 May 1977 (same as Fig. 18).

the squall line shown in Fig. 41. The divergent area may have developed in response to the storm complex over Oklahoma instead of being the cause of it since the divergence field at 1200 GMT (not shown) was relatively flat. A shorter sampling interval (i.e., less than 12 hours) would help to confirm this. The five Oklahoma and Texas tornadoes were located very close to the divergence maximum.

Anticyclonic wind shear was present over the tornado activity with a maximum of -3.2 to -4.8 x 10^{-5} s^{-1} over Kansas (Fig. 45). The area covered by the anticyclonic shear corresponds well with the storm echoes shown in Fig. 41.

A band of moderate PVA (16 to 32 x 10^{-10} s^{-2}) overlaid the Texas-Oklahoma tornadoes (Fig. 46). The remaining tornadoes occurred beneath weak vorticity advection. The distribution of tornado intensity (Fig. 47) reflects this distinction. Of the 5 tornadoes that formed beneath the area of moderate PVA and divergence, 4 were F3 tornadoes and one was F0, but of the tornadoes that formed beneath weak vorticity advection and weak divergence, all were F0 and were more widely scattered. Hence, it appears that the 300-mb dynamics were more favorable for the Texas and Oklahoma tornadoes than for the remainder of the tornadoes. The distributions of 300-mb divergence and PVA in Fig. 48 show much lower average values of PVA and divergence above the tornadoes than in the cases investigated in Sections 3.3 and 3.4.

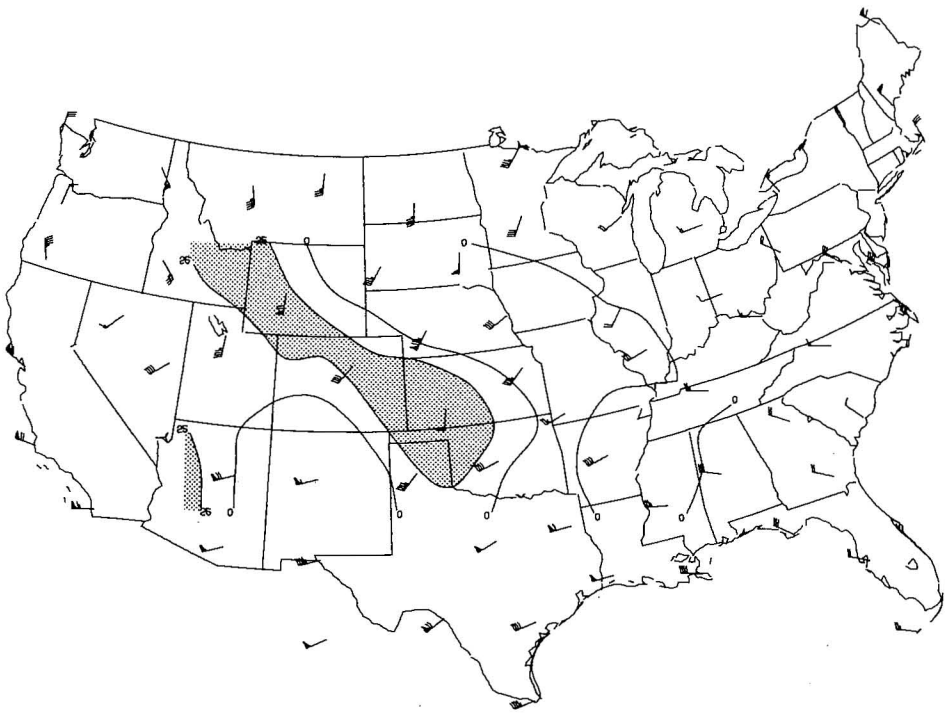

Figure 46. 300-mb positive vorticity advection for 0000 GMT 17 May 1977 (same as Fig. 19).

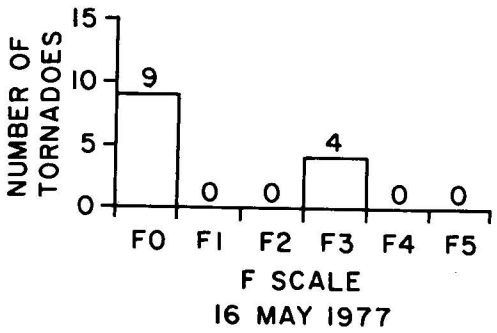

Figure 47. Histogram of tornado F scales for 16 May 1977.

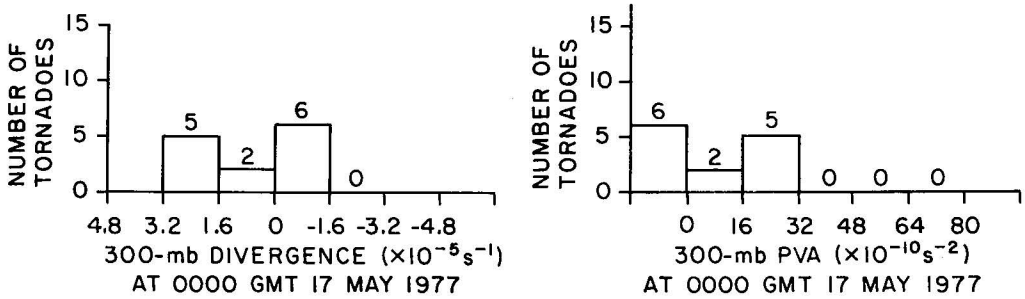

(a) (b)

Figure 48. Distributions of 300-mb (a) divergence and (b) PVA values above tornadoes for 0000 GMT 17 May 1977.

3.6 Synthesis of Case Study Results

In all cases, the tornadoes occurred in diffluent 300-mb flow in regions of weak relative vorticity with a vorticity maximum well to the west of the tornado activity. The composite maps at 1200 GMT (9 to 15 hours prior to the tornadoes) show that the tornadoes generally occurred within the region of 850-mb moisture and strong winds, and within a few hundred kilometers of surface fronts. The radar summary charts show that many (but not all) of the intense thunderstorms were located in regions of 300-mb divergence and positive vorticity advection.

On the four days studied there were between 13 and 17 tornadoes, but differences in average tornado intensity and organization of the activity were noted between cases. On 20 May, the 300-mb kinematics (divergence and PVA) were strongest, the activity occurred as a well organized progressive outbreak, and the tornadoes on the average were more intense than on the other days. In contrast, the upper-level (synoptic-scale) features were weak on 16 May and the activity was widely scattered over a large area. On the other two days, the 300-mb divergence and PVA was of moderate strength, and the activity, although of comparable intensity to 16 May, was organized as either a progressive (4 May) or a line (18 May) outbreak. Examination of the other five days shows general agreement with these findings.

Several tornadoes occurred close to the maxima of 300-mb divergence and PVA while many others occurred in the regions of divergence and PVA gradients rather than within the maximum isopleths. However, this is to be expected for several reasons as follows:

i) The area within the maximum isopleth is small compared to the area of gradient so that, even if the per unit area tornado frequency is highest within the maximum isopleth, it is not surprising that most tornadoes fall within the gradient region.

ii) A perfect match between the maxima and tornado events should not be expected because the maxima may move considerable distances during the ±3 hour time window encompassing the tornado reports.

iii) A perfect match is also unlikely because other key parameters such as instability and low-level convergence probably have maxima at other locations, and it is a combination of low- and upper-level features which determines the area of maximum tornado threat. In extreme cases, the atmospheric stratification may be so unstable that low-level convergence alone (without superposition of upper-level divergence) may be sufficient to trigger severe weather.

iv) Mesoscale divergence and PVA regions, such as those associated with jetlets,[2] may be present without being detected by the network.

Thus, there is no convincing evidence to support McNulty's (1978) conclusion that weak to moderate values of synoptic scale vertical velocity, upper-level divergence, and PVA favor tornado formation more than strong values. In fact, high values of 300-mb divergence and PVA were associated with the 20 May outbreak.

4. SUMMARY AND CONCLUDING REMARKS

Objective analysis of 300-mb wind data for 0000 GMT revealed dynamic features not obvious in the basic flow field. Fields of divergence, relative vorticity, horizontal shear, and vorticity advection were generated. When the locations of the tornadoes which occurred at 0000 GMT ±3 hours were superimposed onto these analyses, the result was a representative picture of the 300-mb synoptic conditions near tornado time. This helped to establish which 300-mb conditions were favorable for tornado occurrence in the central United States during May 1977. The findings are summarized below.

a) Tornadoes generally occurred beneath 300-mb winds of 15 to 35 m s^{-1}, within 1250 km of a 300-mb jet streak whose maximum winds were 35 to 55 m s^{-1} and in the left front or right rear quadrant of the jet streak. The majority of tornadoes were F0 or F1 intensity.

b) The association of 300-mb divergence with tornadoes was statistically significant ($\alpha = .05$). Hence, 300-mb divergence favors tornado development more than 300-mb convergence. However, no correlation between 300-mb divergence and tornado intensity (F scale) was detected. The divergence values obtained in this

[2] Jetlets are small regions of jet-strength wind.

study were considerably larger than those found by McNulty (1978), probably because the objective analysis scheme used here did not dampen the shorter waves so much.

c) Horizontal wind shear at 300 mb was shown not to be a significant parameter for overall tornado occurrence. However, there was a tendency for weak tornadoes (F0) to be associated with anticyclonic shear and stronger tornadoes ($\geq$F1) to be associated with cyclonic shear. This is contrary to the results obtained by Hales (1979).

d) The association of 300-mb positive vorticity advection (PVA) with tornado occurrence was found to be statistically significant (α = .05). Thus, areas of 300-mb PVA are more favorable for tornado development than NVA areas. No correlation between PVA and tornado intensity was found at the 5% level of significance. Further statistical analysis revealed a strong relationship between 300-mb divergence and PVA. This was not unexpected since it was previously demonstrated (Section 1.2) that divergence and PVA are related theoretically.

e) Most tornadoes occurred beneath areas of fairly weak 300-mb relative vorticity ($<4.8 \times 10^{-5}$ s^{-1}). Hence, regions of maximum relative vorticity are not favorable for tornado occurrence. This result is reasonable since upward motion tends to be associated with PVA and decreasing 300-mb relative vorticity (Section 1.2).

f) The most frequent combination of 300-mb conditions for tornado occurrence was divergence and PVA which accounted for 56 of the 96 tornadoes studied.

g) The intensity and combination of the 300-mb parameters may affect the pattern of tornado events, i.e., isolated versus outbreak or widespread versus limited area of tornado activity. The more dynamically favored an area was at 300 mb, the more organized and intense the tornado activity seemed to be.

h) Although 143 tornadoes were included in the data set, this sample was generally insufficient to detect correlations between tornado intensity and 300-mb flow features. The difficulty in establishing statistically significant associations between tornado intensity and flow parameters arises because strong tornadoes are rare and not enough were sampled (only 25 were F2 or stronger). Obtaining a sample with a sufficient number of intense tornadoes would require a much larger data base and considerable resources.

Note that the above conclusions are valid for the synoptic scale. Since jet streaks are generally meso-α scale phenomena, finer resolution (i.e., smaller station spacing) would improve data quality. Jetlets may be completely undetected by the synoptic scale rawinsonde network. Analysis of the SESAME '79 regional scale data would help verify some of the conclusions drawn from this study. For instance, divergence and PVA might be even more significant in finer-scale analyses.

Since PVA and divergence are usually stronger at 300-mb than at 500 mb (because the 500-mb surface is closer to the level of non-divergence (Hales, 1979)), 300-mb forecast divergence and PVA fields from operational numerical models might aid the severe storm forecaster considerably. At present, 300-mb forecast maps are transmitted only over FOFAX[3] and contain just the height contours and isotachs.

Finally, the reader should recall that the 300-mb level is not the only important level for determining tornado potential. The 300-mb level should be examined in association with other levels so that all important weather forecasting parameters are considered in pinpointing the maximum threat area. In particular, conditional and convective instability, low-level jets, low-level convergence, sufficient moisture in the lowest 100 mb of the atmosphere, and low to mid-level dry intrusions are generally present in severe weather outbreaks in addition to upper-level divergence and positive vorticity advection. Surface charts should be examined for mesoscale features such as moist tongues which may be undetected by the rawinsonde network but may play a critical role in the development of severe weather in cases where the synoptic scale instability field is marginal.

4. ACKNOWLEDGMENTS

The work presented here was submitted by Carolyn M. Kloth in partial fulfillment of requirements for the degree of Master of Science at the University of Oklahoma. Thanks go to Drs. Rex Inman and Jeff Kimpel of the University of Oklahoma for their comments and review of this manuscript.

We are sincerely grateful for broad-based support at NSSL. Many thanks go to Mike Weible for his computer programming assistance, to Joan Kimpel and Charles Clark for their graphics support, and especially to Sandy Mudd for her patience and skill in typing this paper. Thanks also to Steve Nelson, Rodger Brown, and Dr. Ken Johnson for their helpful suggestions and moral support.

We are indebted to Horace Hudson of the National Severe Storms Forecast Center in Kansas City, Missouri, for his help in obtaining rawinsonde data for this research.

Lastly, Carolyn Kloth wishes to thank Drs. Edwin Kessler and Ronnie Alberty of NSSL for enabling her to participate in the Environmental Research Laboratory's Graduate COOP Program.

[3]FOFAX is an acronym for the Forecaster's Facsimile circuit.

REFERENCES

Achtemeier, G. L., 1979: Evaluation of operational objective streamline methods. Mon. Wea. Rev., 107, 198-206.

Beebe, R. G., and F. C. Bates, 1955: A mechanism for assisting in the release of convective instability. Mon. Wea. Rev., 83, 1-10.

Cressman, G. P., 1959: An operational objective analysis system. Mon. Wea. Rev., 87, 367-374.

Dickson, R. R., 1977: Weather and circulation of May 1977. Mon. Wea. Rev., 105, 1075-1080.

Emanuel, K. A., 1978: Inertial instability and mesoscale convective systems. Ph.D. Thesis, Dept. of Meteorology, Mass. Inst. of Tech., 207 pp.

Fawbush, E. J., R. C. Miller, and L. G. Starrett, 1951: An empirical method of forecasting tornado development. Bull. Amer. Meteor. Soc., 32, 1-9.

Fujita, T. T., 1971: Proposed characterization of tornadoes and hurricanes by area and intensity. Satellite and Mesometeorology Research Project, Research Paper No. 91, Dept. of the Geophysical Sciences, Univ. of Chicago.

Galway, J. G., 1977: Some climatological aspects of tornado outbreaks. Mon. Wea. Rev., 105, 477-484.

Hales, J. E., Jr., 1979: On the relationship of 250 mb positive vorticity advection and horizontal divergence to tornado and severe thunderstorm development. Preprints, 11th Conf. on Severe Local Storms, Kansas City, MO, Amer. Meteor. Soc., 28-31.

Haltiner, G. J., 1971: Numerical Weather Prediction. John Wiley & Sons, Inc., New York, 317 pp.

Holton, J. R., 1972: Introduction to Dynamic Meteorology. Academic Press, New York, 107-115.

Horn, L. H., and T. H. Achtor, 1979: The mean upper tropospheric jet streak, associated low level jet and static stability for spring season Colorado cyclones. Preprints, 11th Conf. on Severe Local Storms, Kansas City, MO, Amer. Meteor. Soc., 104-107.

House, D. C., 1958: Air mass modification and upper level divergence. Bull. Amer. Meteor. Soc., 39, 137-143.

Huschke, R. E., Ed., 1959: Glossary of Meteorology. Amer. Meteor. Soc., Boston, 323-324.

Inman, R. L., 1970: Papers on operational objective analysis schemes at the National Severe Storms Forecast Center. NOAA Tech. Memo. ERL-NSSL 51, National Severe Storms Lab., Norman, Okla. 91 pp.

Karst, O. J., 1977: Thunderstorm development in a jet stream diffluence zone. Nat. Wea. Dig., 2, 10-13.

Lee, J. T., and J. G. Galway, 1956: Preliminary report on the relationship between the jet at the 200 mb level and tornado occurrence. Bull. Amer. Meteor. Soc., 37, 327-332.

___, and J. G. Galway, 1958: The jet chart. Bull. Amer. Meteor. Soc., 39, 217-223.

Maddox, R. A., 1979: The evolution of middle and upper tropospheric features during a period of intense convective storms. Preprints, 11th Conf. on Severe Local Storms, Kansas City, MO, Amer. Meteor. Soc., 41-48.

McIntosh, D. H., Ed., 1972: Meteorological Glossary. Chemical Publishing Co., New York, 160.

McNulty, R. P., 1978: On upper tropospheric kinematics and severe weather occurrence. Mon. Wea. Rev., 106, 662-672.

Miller, R. C., 1972: Notes on analysis and severe storm forecasting procedures of the Air Force Global Weather Central. Tech. Rep. 200 (Rev), Air Weather Service, U. S. Air Force, 190 pp. [Available Scott AFB, Ill.]

Newton, C. W., 1959: Axial velocity streaks in the jet stream: ageostrophic "inertial" oscillations. J. Meteor., 16, 638-645.

_____, and E. Palmén, 1963: Kinematic and thermal properties of a large-amplitude wave in the westerlies. Tellus, 15, 99-119.

Pautz, M. E., 1969: Severe local storm occurrences, 1955-1967. ESSA Tech. Memo. WBTM FCST 12, U.S. Weather Bureau, Silver Spring, MD, 77 pp.

Petterssen, S., 1956: Weather Analysis and Forecasting, Vol. 1 (2nd Ed.), McGraw-Hill, New York, 428 pp.

Reiter, E. R., 1967: Jet Streams. Doubleday & Co., Inc., New York, 178 pp.

Riehl, H., M. A. Alaka, C. L. Jordan, and R. J. Renard, 1954: The Jetstream. Meteor. Monogr., 2, No. 7, 54 pp.

Saucier, W. J., 1956: Principles of Meteorological Analysis. Univ. of Chicago, Chicago, IL, 438 pp.

Sechrist, F. S., and T. M. Whittaker, 1979: Evidence of jet streak vertical circulations. Mon. Wea. Rev., 107, 1015-1021.

Shuman, F. G., 1957: Numerical methods in weather prediction: II Smoothing and filtering. Mon. Wea. Rev., 85, 359-361.

Stephens, J. J., and A. L. Polan, 1971: Spectral modification by objective analysis. Mon Wea. Rev., 99, 374-378.

Uccellini, L. W., and D. R. Johnson, 1979: The coupling of upper and lower tropospheric jet streaks and implications for the development of severe convective storms. Mon. Wea. Rev., 107, 682-703.

U.S. Dept. of Commerce, 1977a: Climatological Data, National Summary. Environmental Data Service, NOAA, National Climatic Center, Asheville, NC, 28, No. 5.

_____, 1977b: Daily Weather Maps. Environmental Data Service, NOAA, National Climatic Center, Asheville, NC.

_____, 1977c: Storm Data. Environmental Data Service, NOAA, National Climatic Center, Asheville, NC, 19, No. 5.

Whitney, L. F., 1977: Relationship of the sub-tropical jet stream to severe storms. Mon. Wea. Rev., 105, 398-412.

Yamane, T., 1973: Statistics: An Introductory Analysis. (3rd Ed.), Harper & Row, New York, 761-789.

APPENDIX A

THE OBJECTIVE ANALYSIS ROUTINE

APPENDIX A

THE OBJECTIVE ANALYSIS ROUTINE

To compute the parameters pertinent to this investigation, a general purpose objective analysis routine was developed.

No attempt was made to edit the 300-mb data from NSSFC's RAOB History tape for errors within the program itself. Instead, any blatant errors that appeared in individual runs were edited manually. Data from 73 rawinsonde stations (71 NWS upper air stations within the continental United States plus 2 Mexican stations, Chihuahua and Empalmé) were used.

A polar stereographic projection was used with true latitude 90°N, true longitude 106°W, and map factor 1:20,600,000 (Inman, 1970). The station distribution was relatively uniform with an average spacing of about 310 km (at 40°N) or 0.72 inches on the map. Following Stephens and Polan (1971), a circular radius of influence equal to 1.75 times the average station spacing was utilized. The radius of influence was kept constant throughout due to the uniformity of the data density.

A 17 x 11 grid with 1/2 inch spacing between grid points (215 km at 40°N) was employed. The lower left-hand corner of the grid, (x_1, y_1) was placed at 29.3° N latitude, 116.3° W longitude so that the boundaries of the grid were located just inside the outermost stations (see Fig. A1). This grid allowed the data from all the stations to be used in each pass and minimized extrapolation errors along the boundaries due to lack of data.

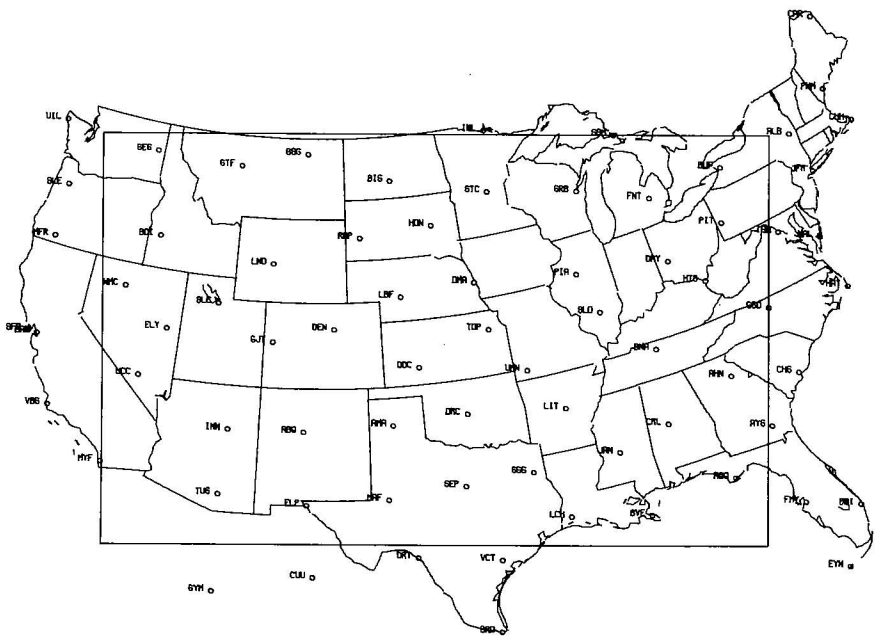

Figure A1. Rawinsonde stations in United States and Mexico from which data was obtained. Rectangle indicates outer boundary of the objective analysis grid.

A simple successive corrections scheme was implemented to provide a series of corrections to initial estimates at each grid point. The initial guess field at each grid point was the average value of the field being analyzed, and was computed in the main program from the data at all available stations.

Following Cressmen (1959), the weight function is defined as

$$W_k = \frac{R^2 - d_k^2}{R^2 + d_k^2} \quad , \quad \text{for } d_k < R \quad , \tag{A.1}$$

$$W_k = 0 \quad , \quad \text{for } d_k \geq R \quad ,$$

where R is the radius of influence and d_k is the distance of the k^{th} station from the grid point under consideration.

The formula for the successive corrections scheme is

$$\overset{*}{Z}{}^{\mu}_{i,j} = \overset{*}{Z}{}^{\mu-1}_{i,j} + C^{\mu}_{i,j} \quad , \tag{A.2}$$

where $\overset{*}{Z}{}^{\mu-1}_{i,j}$ is the value at the grid point from the previous pass, $\overset{*}{Z}{}^{\mu}_{i,j}$ is the new value at the grid point, and $C^{\mu}_{i,j}$ is the correction to the old value, given by

$$C^{\mu}_{i,j} = \frac{\sum_{k=1}^{n} W_k \left| Z_k - \hat{Z}_k^{\mu-1} \right|}{\sum_{k=1}^{n} W_k} \quad . \tag{A.3}$$

In (A.3) Z_k is the observed value at the k^{th} station, $Z_k^{\mu-1}$ is the value at the k^{th} station obtained from bi-linear interpolation of the grid values obtained on the last pass, and n is the number of stations within the radius of influence of the grid point under consideration. On the first pass, all $\hat{Z}_k^0$ were set to the average value of the field being analyzed. On all other passes, $\hat{Z}_k^{\mu}$ was computed by using the value at the four surrounding grid points and interpolating a new value at the station as follows (refer to Fig. A2):

$$\hat{Z}_k^{\mu} = \overset{*}{Z}{}^{\mu}_{r,s} + (\overset{*}{Z}{}^{\mu}_{r,s+1} - \overset{*}{Z}{}^{\mu}_{r,s}) \frac{\delta y_k}{\Delta y} + (\overset{*}{Z}{}^{\mu}_{r+1,s} - \overset{*}{Z}{}^{\mu}_{r,s}) \frac{\delta x_k}{\Delta x} \tag{A.4}$$

$$- (\overset{*}{Z}{}^{\mu}_{r+1,s} - \overset{*}{Z}{}^{\mu}_{r+1,s+1} + \overset{*}{Z}{}^{\mu}_{r,s+1} - \overset{*}{Z}{}^{\mu}_{r,s}) \frac{\delta x_k}{\Delta x} \frac{\delta y_k}{\Delta y} \quad .$$

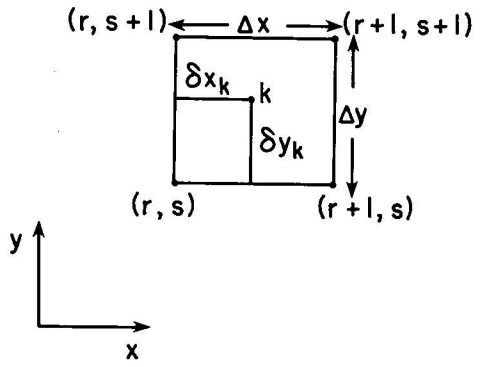

Figure A2. Bi-linear interpolation scheme employed in the objective analysis routine. Indices r and s are directed along the x- y-axes, respectively; Δx and Δy are distances between grid points in the x- and y-directions, respectively; δx_k and δy_k are the distances along the x- and y-axes, respectively, from the lower left grid point (r,s) to the station k.

For stations outside the grid, the new value for $\hat{Z}_k^{\mu}$ on each pass was computed in the same manner as the value at a grid point. That is,

$$\hat{Z}_e^{\mu} = \hat{Z}_e^{\mu-1} + C_e^{\mu} \quad , \tag{A.5}$$

where

$$C_e^{\mu} = \frac{\sum_{k=1}^{n} W_k' \left[Z_k - \hat{Z}_k^{\mu-1} \right]}{\sum_{k=1}^{n} W_k'} \quad , \tag{A.6}$$

and where W_k', the Cressman weight function, is now defined as

$$W_k' = \frac{R^2 - d_{e,k}^2}{R^2 + d_{e,k}^2} \quad . \tag{A.7}$$

e, under consideration and the k^{th} station. The sum is over all stations within the radius of influence.

The values at all the grid points were then smoothed using a three-point Shuman (1957) filter of the form

$$\overline{Z}_j = (1-S)Z_j + S(Z_{j+1} + A_{j-1})/2 \quad , \tag{A.8}$$

where Z_j is the value at the j^{th} grid point, $\overline{Z}_j$ is the smoothed value at the j^{th} grid point, and S determines the weight given to each grid point value. The smoothing operator was applied first in the x-direction, then in the y-direction since it has been shown by Shuman (1957) that the final result is independent of the directional order in which the smoothing is applied.

The response function, σ, is the ratio of the smoothed to the unsmoothed value, and is computed as a function of wavelength as follows. Let $Z_j = Ze^{ikx}$ where $x = j\Delta x$, $k = \frac{2\pi}{L}$, and L = wavelength. Then,

$$\overline{Z}_j = (1-S)Ae^{ikj\Delta x} + S(Ae^{ik(j+1)\Delta x} + Ae^{ik(j-1)\Delta x})/2$$

$$= (1-S)Ae^{ikj\Delta x} + S(e^{ik\Delta x} + e^{-ik\Delta x})Ae^{ikj\Delta x}/2 \quad ;$$

i.e.,

$$\overline{Z}_j = (1-S)Z_j + S(e^{ik\Delta x} + e^{-ik\Delta x})Z_j/2 \quad .$$

Thus,

$$\sigma = \frac{\overline{Z}_j}{Z_j} = 1-S + S(2\cos k\Delta x)/2 = 1 - S\,(1 - \cos k\Delta x) \quad ,$$

since from Euler's formula: $\cos x = (e^{ix} + e^{-ix})/2$.

Thus, this particular smoothing operator does not affect the wave number or phase of the wave (provided $\sigma \geq 0$), but only its amplitude. If $|\sigma| > 1$, the wave is amplified by the operation, while $|\sigma| < 1$ results in damping (Haltiner, 1971).

Shuman has shown that successive application of several smoothing operators with weights $S_0, S_1, \ldots S_n$ results in a final response function of

$$\sum = \sigma_0\sigma_1\ldots\sigma_n = \prod_{i=1}^{n} [1 - S_i(1-\cos k\Delta x)] \quad .$$

Here, two successive applications of the smoothing operator were used, first with S = 0.5, then with S = -0.5. This allows a better frequency response for wavelengths greater than $4\Delta x$ (compared to the frequency response for one application with S = 0.5) while at the same time still suppressing wavelengths less than or equal to $4\Delta x$ (see Figs. A3a-A3c).

The number of passes made through the objective analysis routine was determined by observing how much detail was retained with each pass. Since changes were minor after four passes, four passes were made for each analysis.

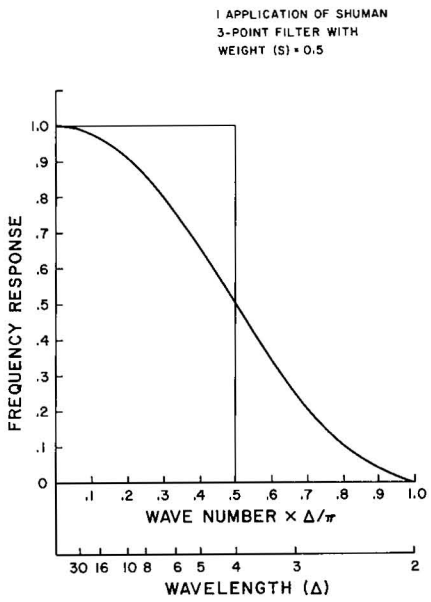

(a)

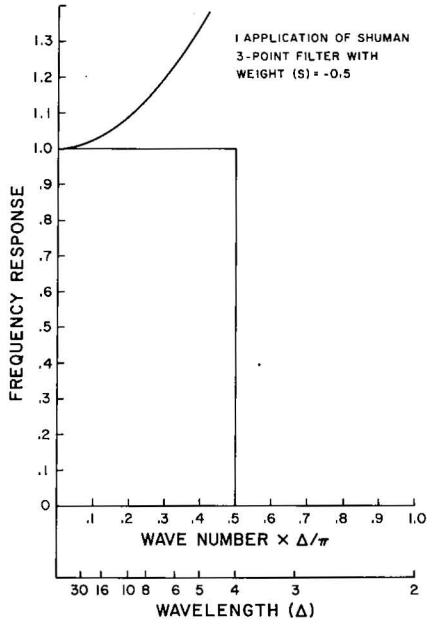

(b)

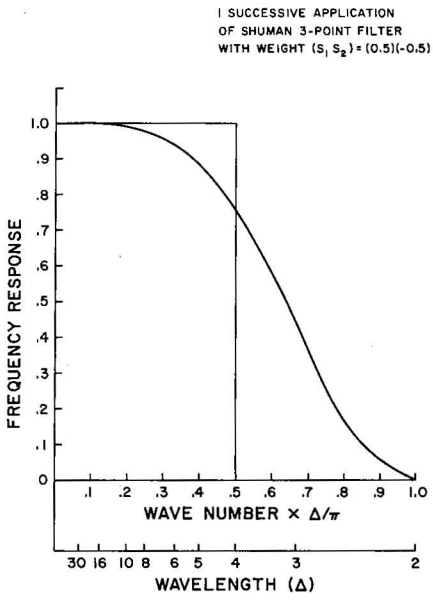

(c)

Figure A3. Response functions for one application of a Shuman three-point filter with (a) weight $S = 0.5$, (b) weight $s = -0.5$, and (c) weight $S = S_o S_1 = (0.5)(-0.5)$.

NATIONAL SEVERE STORMS LABORATORY

The NSSL Technical Memorandum, beginning with No. 28, continue the sequence established by the U. S. Weather Bureau National Severe Storms Project, Kansas City, Missouri. Numbers 1-22 were designated NSSP Reports. Numbers 23-27 were NSSL Reports, and 24-27 appeared as subseries of Weather Bureau Technical Notes. These reports are available from the National Technical Information Service, Operations Division, Springfield, Virginia 22151, a microfiche version for $3.50 or a hard copy, cost depending upon the number of pages. NTIS numbers are given below in parenthesis.

No. 1 National Severe Storms Project Objectives and Basic Design. Staff, NSSP. March 1961, 16 p. (PB-168207)

No. 2 The Development of Aircraft Investigations of Squall Lines from 1956-1960. B. B. Goddard. 34 p. (PB-168208)

No. 3 Instability Lines and Their Environments as Shown by Aircraft Soundings and Quasi-Horizontal Traverses. D. T. Williams. February 1962. 15 p. (PB-168209)

No. 4 On the Mechanics of the Tornado. J. R. Fulks. February 1962. 33 p. (PB-168210)

No. 5 A Summary of Field Operations and Data Collection by the National Severe Storms Project in Spring 1961. J. T. Lee. March 1962. 47 p. (PB-165095)

No. 6 Index to the NSSP Surface Network. T. Fujita. April 1962. 32 p. (PB-168212)

No. 7 The vertical structure of Three Dry Lines as Revealed by Aircraft Traverses. E. L. McGuire. April 1962. 10 p. (PB-168213)

No. 8 Radar Observations of a Tornado Thunderstorm in Vertical Section. Ralph J. Donaldson, Jr. April 1962. 21 p. (PB-174859)

No. 9 Dynamics of Severe Convective Storms. Chester W. Newton. July 1962. 44 p. (PB-163319)

No. 10 Some Measured Characteristics of Severe Storms Turbulence. Roy Steiner and Richard H. Rhyne. July 1962. 17 p. (N62-16401)

No. 11 A Study of the Kinematic Properties of Certain Small-Scale Systems. D. T. Williams. October 1962. 22 p. (PB-168216)

No. 12 Analysis of the Severe Weather Factor in Automatic Control of Air Route Traffic. W. Boynton Beckwith. December 1962. 67 p. (PB-168217)

No. 13 500-Kc./Sec. Sferics Studies in Severe Storms. Douglas A. Kohl and John E. Miller. April 1963. 36 p. (PB-168218)

No. 14 Field Operations of the National Severe Storms Project in Spring 1962. L. D. Sanders. May 1963. 71 p. (PB-168219)

No. 15 Penetrations of Thunderstorms by an Aircraft Flying at Supersonic Speeds. G. P. Roys. Radar Photographs and Gust Loads in Three Storms of 1961 Rough Rider. Paul W. J. Schumacher. May 1963. 19 p. (PB-168220)

No. 16 Analysis of Selected Aircraft Data from NSSP Operations, 1962. T. Fujita. May 1963. 29 p. (PB-168221)

No. 17 Analysis of Methods for Small-Scale Surface Network Data. D. T. Williams. August 1963. 20 p. (PB-168222)

No. 18 The Thunderstorm Wake of May 4, 1961. D. T. Williams. August 1963. 23 p. (PB-168223)

No. 19 Measurements by Aircraft of Condensed Water in Great Plains Thunderstorms. George P. Roys and Edwin Kessler. July 1966. 17 p. (PB-173048)

No. 20 Field Operations of the National Severe Storms Project in Spring 1963. J. T. Lee, L. D. Sanders, and D. T. Williams. January 1964. 68 p. (PB-168224)

No. 21 On the Motion and Predictability of Convective Systems as Related to the Upper Winds in a Case of Small Turning of Wind with Height. James C. Fankhauser. January 1964. 36 p. (PB-168225)

No. 22 Movement and Development Patterns of Convective Storms and Forecasting the Probability of Storm Passage at a Given Location. Chester W. Newton and James C. Fankhauser. January 1964. 53 p. (PB-168226)

No. 23 Purposes and Programs of the National Severe Storms Laboratory, Norman, Oklahoma. Edwin Kessler. December 1964. 17 p. (PB-166675)

No. 24 Papers on Weather Radar, Atmospheric Turbulence, Sferics and Data Processing. August 1965. 139 p. (AD-621586)

No. 25 A Comparison of Kinematically Computed Precipitation with Observed Convective Rainfall. James C. Fankhauser. September 1965. 28 p. (PB-168445)

No. 26 Probing Air Motion by Doppler Analysis of Radar Clear Air Returns. Roger M. Lhermitte. May 1966. 37 p. (PB-170636)

No. 27 Statistical Properties of Radar Echo Patterns and the Radar Echo Process. Larry Armijo. May 1966. The Role of the Kutta-Joukowski Force in Cloud Systems with Circulation. J. L. Goldman. May 1966. 34 p. (PB-170756)

No. 28 Movement and Predictability of Radar Echoes. James Warren Wilson. November 1966. 30 p. (PB-173972)

No. 29 Notes on Thunderstorm Motions, Heights, and Circulations. T. W. Harrold, W. T. Roach, and Kenneth E. Wilk. November 1966. 51 p. (AD-644899)

No. 30 Turbulence in Clear Air Near Thunderstorms. Anne Burns, Terence W. Harrold, Jack Burnham, and Clifford S. Spavins. December 1966. 20 p. (PB-173992)

No. 31 Study of a Left-Moving Thunderstorm of 23 April 1964. George R. Hammond. April 1967. 75 p. (PB-174681)

No. 32 Thunderstorm Circulations and Turbulence from Aircraft and Radar Data. James C. Fankhauser and J. T. Lee. April 1967. 32 p. (PB-174860)

No. 33 On the Continuity of Water Substance. Edwin Kessler. April 1967. 125 p. (PB-175840)

No. 34 Note on the Probing Balloon Motion by Doppler Radar. Roger M. Lhermitte. July 1967. 14 p. (PB-175930)

No. 35 A Theory for the Determination of Wind and Precipitation Velocities with Doppler Radars. Larry Armijo. August 1967. 20 p. (PB-176376)

No. 36 A Preliminary Evaluation of the F-100 Rough Rider Turbulence Measurement System. U. O. Lappe. October 1967. 25 p. (PB-177037)

No. 37 Preliminary Quantitative Analysis of Airborne Weather Radar. Lester P. Merritt. December 1967. 32 p. (PB-177188)

No. 38 On the Source of Thunderstorm Rotation. Stanley L. Barnes. March 1968. 28 p. (PB-178990)

No. 39 Thunderstorm - Environment Interactions Revealed by Chaff Trajectories in the Mid-Troposphere. James C. Fankhauser. June 1968. 14 p. (PB-179659)

No. 40 Objective Detection and Correction of Errors in Radiosonde Data. Rex L. Inman. June 1968. 50 p. (PB-180284)

No. 41 Structure and Movement of the Severe Thunderstorms of 3 April 1964 as Revealed from Radar and Surface Mesonetwork Data Analysis. Jess Charba and Yoshikazu Sasaki. October 1968. 47 p. (PB-183310)

No. 42 A Rainfall Rate Sensor. Brian E. Morgan. November 1968. 10 p. (PB-183979)

No. 43 Detection and Presentation of Severe Thunderstorms by Airborne and Ground-based Radars: A Comprehensive Study. Kenneth E. Wilk, John K. Carter, and J. T. Dooley. February 1969. 56 p. (PB-183572)

No. 44 A Study of a Severe Local Storm of 16 April 1967. George Thomas Haglund. May 1969. 54 p. (PB-184970)

No. 45 On the Relationship Between Horizontal Moisture Convergence and Convective Cloud Formation. Horace R. Hudson. March 1970. 29 p. (PB-191720)

No. 46 Severe Thunderstorm Radar Echo Motion and Related Weather Events Hazardous to Aviation Operations. Peter A. Barclay and Kenneth E. Wilk. June 1970. 63 p. (PB-192498)

No. 47 Evaluation of Roughness Lengths at the NSSL-WKY Meteorological Tower. Leslie D. Sanders and Allen H. Weber. August 1970. 24 p. (PB-194587)

No. 48 Behavior of Winds in the Lowest 1500 ft in Central Oklahoma: June 1966-May 1967. Kenneth C. Crawford and Horace R. Hudson. August 1970. 57 p. (N71-10615)

No. 49 Tornado Incidence Maps. Arnold Court. August 1970. 76 p. (COM-71-00019)

No. 50 The Meteorologically Instrumented WKY-TV Tower Facility. John K. Carter. September 1970. 18 p. (COM-71-00108)

No. 51 Papers on Operational Objective Analysis Schemes at the National Severe Storms Forecast Center. Rex L. Inman. November 1970. 91 p. (COM-71-00136)

No. 52 The Exploration of Certain Features of Tornado Dynamics Using a Laboratory Model. Neil B. Ward. November 1970. 22 p. (COM-71-00139)

No. 53 Rawinsonde Observation and Processing Techniques at the National Severe Storms Laboratory. Stanley L. Barnes, James H. Henderson and Robert J. Ketchum. April 1971. 245 p. (COM-71-00707)

No. 54 Model of Precipitation and Vertical Air Currents. Edwin Kessler and William C. Bumgarner. June 1971. 93 p. (COM-71-00911)

No. 55 The NSSL Surface Network and Observations of Hazardous Wind Gusts. Operations Staff. June 1971. 20 p. (COM-71-00910)

No. 56 Pilot Chaff Project at the National Severe Storms Laboratory. Edward A. Jessup. November 1971. 36 p. (COM-72-10106)

No. 57 Numerical Simulation of Convective Vortices. Robert P. Davies-Jones and Glenn T. Vickers. November 1971. 27 p. (COM-72-10269).

No. 58 The Thermal Structure of the Lowest Half Kilometer in Central Oklahoma: December 9, 1966-May May 31, 1967. R. Craig Goff and Horace R. Hudson. July 1972. 53 p. (COM-72-11281)

No. 59 Cloud-to-Ground Lightning Versus Radar Reflectivity in Oklahoma Thunderstorms. Gilbert D. Kinzer. September 1972. 24 p. (COM-73-10050)

No. 60 Simulated Real Time Displays of Velocity Fields by Doppler Radar. L. D. Hennington and G. B. Walker. November 1972. 10 p. (COM-73-10515)

No. 61 Gravity Current Model Applied to Analysis of Squall-Line Gust Front. Jess Charba. November 1972. 58 p. (COM-73-10410)

No. 62 Mesoscale Objective Map Analysis Using Weighted Time-Series Observations. Stanley L. Barnes. March 1973. 60 p. (COM-73-10781)

No. 63 Observations of Severe Storms on 26 and 28 April 1971. Charles L. Vlcek. April 1973. 19 p. (COM-73-11200)

No. 64 Meteorological Radar Signal Intensity Estimation. Dale Sirmans and R. J. Doviak. September 1973. 80 p. (COM-73-11923/2AS)

No. 65 Radisonde Altitude Measurement Using Double Radiotheodolite Techniques. Stephan P. Nelson. September 1973. 20 p. (COM-73-11932/9AS)

No. 66 The Motion and Morphology of the Dryline. Joseph T. Schaefer. September 1973. 81 p. (COM-74-10043)

No. 67 Radar Rainfall Pattern Optimizing Technique. Edward A. Brandes. March 1974. 16 p. (COM-74-10906/AS)

No. 68 The NSSL/WKY-TV Tower Data Collection Program: April-July 1972. R. Craig Goff and W. David Zittel. May 1974. 45 p. (COM-74-11334/AS)

No. 69 Papers on Oklahoma Thunderstorms, April 29-30, 1970. Stanley L. Barnes, Editor. May 1974. 147 p. (COM-74-11474/AS)

No. 70 Life Cycle of Florida Key's Waterspouts. Joseph H. Golden. June 1974. 147 p. (COM-74-11477/AS)

No. 71 **Interaction of Two Convective Scales Within a Severe Thunderstorm: A Case Study and Thunderstorm** Wake Vortex Structure and Aerodynamic Origin. Leslie R. Lemon. June 1974. 43 p. (COM-74-11642/AS)

No. 72 Updraft Properties Deduced from Rawinsoundings. Robert P. Davies-Jones and James H. Henderson. October 1974. 117 p. (COM-75-10583/AS)

No. 73 Severe Rainstorm at Enid, Oklahoma - October 10, 1973. L. P. Merritt, K. E. Wilk, and M. L. Weible. November 1974. 50 p. (COM-75-10583/AS)

No. 74 Mesonetwork Array: Its Effect on Thunderstorm Flow Resolution. Stanley L. Barnes. October 1974. 16 p. (COM-75-10248/AS)

No. 75 Thunderstorm-Outflow Kinematics and Dynamics. R. Craig Goff. December 1975. 63 p. (PB-250808/AS)

No. 76 An Analysis of Weather Spectra Variance in a Tornadic Storm. Philippe Waldteufel. May 1976. 80 p. (PB-258456/AS)

No. 77 Normalized Indices of Destruction and Deaths by Tornadoes. Edwin Kessler and J. T. Lee. June 1976. 47 p. (PB-260923/AS)

No. 78 Objectives and Accomplishments of the NSSL 1975 Spring Program. K. Wilk, K. Gray, C. Clark, D. Sirmans, J. Dooley, J. Carter, and W. Bumgarner. July 1976. 47 p. (PB-263813/AS)

No. 79 Subsynoptic Scale Dynamics As Revealed By The Use Of Filtered Surface Data. Charles A. Doswell III. December 1976. 40 p. (PB-265433/AS)

No. 80 The Union City, Oklahoma Tornado of 24 May 1973. Rodger A. Brown, Editor. December 1976. 235 p. (PB-269443/AS)

No. 81 Mesocyclone Evolution and Tornado Generation Within the Harrah, Oklahoma Storm. Edward A. Brandes. May 1977 28 p. (PB-271675/AS)

No. 82 The Tornado: An Engineering-Oriented Perspective. Joseph E. Minor, James R. McDonald, and Kishor C. Mehta. December 1977. 196 p. (PB-281860/AS)

No. 83 Spring Program '76. R. L. Alberty, J. F. Weaver, D. Sirmans, J. T. Dooley, and B. Bumgarner. December 1977. 130 p. (PB280745/AS)

No. 84 Spring Program '77. P. S. Ray, J. Weaver, and NSSL Staff. December 1977. 173 p. (PB-284953/AS)

No. 85 A Dual-Doppler Variational Objective Analysis as Applied to Studies of Convective Storms. Conrad L. Ziegler. November 1978. 116 p. (PB-293581/AS)

No. 86 Final Report on the Joint Doppler Operational Project (JDOP) 1976-78. Prepared by Staff of the National Severe Storms Laboratory, Environmental Research Laboratories; Weather Radar Branch, Air Force Geophysics Laboratory; Equipment Development Laboratory, National Weather Service; and Air Weather Service, United States Air Force. March 1979. 84 p. (PB80-107180/AS)

No. 87 An Analysis of the Clear Air Planetary Boundary Layer Wind Synthesized from NSSL's Dual Doppler-Radar Data. Myron I. Berger and R. J. Doviak. June 1979. 55 p. (PB-300865/AS)

☆ U. S. GOVERNMENT PRINTING OFFICE: 1980—677-096/1260 REGION NO. 8